

## Original research

# Integrative multiomics enhancer activity profiling identifies therapeutic vulnerabilities in cholangiocarcinoma of different etiologies

Jing Han Hong ,<sup>1</sup> Chern Han Yong,<sup>2,3</sup> Hong Lee Heng,<sup>2</sup> Jason Yongsheng Chan,<sup>4,5,6</sup> Mai Chan Lau,<sup>7,8</sup> Jianfeng Chen,<sup>9</sup> Jing Yi Lee,<sup>2,5</sup> Abner Herbert Lim,<sup>2,5</sup> Zhimei Li,<sup>2,5</sup> Peiyong Guan,<sup>10</sup> Pek Lim Chu,<sup>1</sup> Arnoud Boot,<sup>1,11</sup> Sheng Rong Ng ,<sup>12</sup> Xiaosai Yao,<sup>12</sup> Felicia Yu Ting Wee,<sup>13</sup> Jeffrey Chun Tatt Lim,<sup>13</sup> Wei Liu,<sup>2</sup> Peili Wang,<sup>9</sup> Rong Xiao,<sup>9</sup> Xian Zeng,<sup>9</sup> Yichen Sun,<sup>9</sup> Joanna Koh,<sup>12</sup> Xiu Yi Kwek,<sup>2</sup> Cedric Chuan Young Ng,<sup>2,5</sup> Poramate Klanrit,<sup>14,15</sup> Yaojun Zhang,<sup>9,16</sup> Jiaming Lai,<sup>17</sup> David Wai Meng Tai,<sup>4,6</sup> Chawalit Pairojkul,<sup>18</sup> Simona Dima,<sup>19</sup> Irinel Popescu,<sup>19</sup> Sen-Yung Hsieh,<sup>20</sup> Ming-Chin Yu,<sup>21</sup> Joe Yeong ,<sup>13,22,23</sup> Sarinya Kongpetch,<sup>24,25</sup> Apinya Jusakul,<sup>24,26</sup> Watcharin Loilome,<sup>14,15,24</sup> Patrick Tan ,<sup>1,10,27</sup> Jing Tan ,<sup>2,28</sup> Bin Tean Teh ,<sup>1,2,10,12</sup>

► Additional supplemental material is published online only. To view, please visit the journal online (<http://dx.doi.org/10.1136/gutjnl-2023-330483>).

For numbered affiliations see end of article.

**Correspondence to**  
Professor Bin Tean Teh,  
Laboratory of Cancer  
Epigenome, National Cancer  
Centre Singapore, Singapore;  
teh.bin.tean@singhealth.com.sg

JHH and CHY are joint first authors.

JT and BTT are joint senior authors.

Received 13 June 2023  
Accepted 6 November 2023

## ABSTRACT

**Objectives** Cholangiocarcinoma (CCA) is a heterogeneous malignancy with high mortality and dismal prognosis, and an urgent clinical need for new therapies. Knowledge of the CCA epigenome is largely limited to aberrant DNA methylation. Dysregulation of enhancer activities has been identified to affect carcinogenesis and leveraged for new therapies but is uninvestigated in CCA. Our aim is to identify potential therapeutic targets in different subtypes of CCA through enhancer profiling.

**Design** Integrative multiomics enhancer activity profiling of diverse CCA was performed. A panel of diverse CCA cell lines, patient-derived and cell line-derived xenografts were used to study identified enriched pathways and vulnerabilities. NanoString, multiplex immunohistochemistry staining and single-cell spatial transcriptomics were used to explore the immunogenicity of diverse CCA.

**Results** We identified three distinct groups, associated with different etiologies and unique pathways. Drug inhibitors of identified pathways reduced tumour growth in *in vitro* and *in vivo* models. The first group (ESTRO), with mostly fluke-positive CCAs, displayed activation in estrogen signalling and were sensitive to MTOR inhibitors. Another group (OXPHO), with mostly *BAP1* and *IDH*-mutant CCAs, displayed activated oxidative phosphorylation pathways, and were sensitive to oxidative phosphorylation inhibitors. Immune-related pathways were activated in the final group (IMMUN), made up of an immunogenic CCA subtype and CCA with aristolochic acid (AA) mutational signatures. Intratumour differences in AA mutation load were correlated to intratumour variation of different immune cell populations.

**Conclusion** Our study elucidates the mechanisms underlying enhancer dysregulation and deepens understanding of different tumourigenesis processes in distinct CCA subtypes, with potential significant therapeutics and clinical benefits.

## WHAT IS ALREADY KNOWN ON THIS TOPIC

- ⇒ The etiologies, epidemiology, pathogenesis and risk factors for cholangiocarcinoma (CCA) are diverse; there are lack of effective therapies for the disease and immunotherapy is also known to be largely ineffective for CCA.
- ⇒ Enhancer activity is frequently dysregulated in cancers and affects tumour development and response to therapy.
- ⇒ Studies have shown genome-wide DNA methylation dysregulation in CCA, suggesting similar aberrations in enhancer activities.

## INTRODUCTION

Cholangiocarcinoma (CCA) is the second most frequent liver malignancy, with high incidence in Southeast Asia due to infection by the parasite liver fluke. It is a heterogeneous malignancy with a bleak prognosis. The first-line standard of care for CCA is chemotherapy (eg, gemcitabine), while the second line is targeted therapies or immune checkpoint therapies. Genomic alterations in CCA have been characterised in recent years, and targeted treatments have been approved by the United States Food and Drug Administration (FDA) for a subset of patients with *IDH1* activating mutations and *FGFR2* fusions or rearrangements.<sup>1–3</sup> These only account for roughly 20% of patients diagnosed with intrahepatic CCA of non-fluke etiology.<sup>4,5</sup> However, for most patients, due to its typical late diagnosis, treatment options are more often limited to palliative chemotherapy in the advanced setting. Therefore, effective approaches are still non-existent for the majority of patients. Thus, there is a need for discovery of new therapies to complement existing treatments and to improve the clinical outcomes for these patients.



© Author(s) (or their employer(s)) 2023. No commercial re-use. See rights and permissions. Published by BMJ.

**To cite:** Hong JH, Yong CH, Heng HL, et al. Gut Epub ahead of print: [please include Day Month Year]. doi:10.1136/gutjnl-2023-330483

**WHAT THIS STUDY ADDS**

- ⇒ Integrative multiomics enhancer activity profiling of diverse CCA (including fluke-negative and fluke-positive CCA) identifies 3 three distinct groups of CCAs with unique enriched pathways that can be targeted therapeutically.
- ⇒ The identified unique pathways can be targeted by pharmacological drugs, and the effectiveness of the drugs were successfully validated in a panel of carefully curated diverse CCA cell lines, and patient-derived and cell-line derived xenografts, with tumour growth of CCA from the distinct group suppressed but not the other groups. This shows the specificity and selectivity of the identified pathway and drug for each distinct group of CCA identified.
- ⇒ Inter-group and intra-tumour immunogenicity of CCA tumours were identified using novel technologies including NanoString, multiplex immunohistochemistry staining (Vectra) and single-cell spatial transcriptomics (Visium). Correlation of differences in intratumour microenvironment to intratumour variation in aristolochic acid (AA) mutation signatures load was observed.

**HOW THIS STUDY MIGHT AFFECT RESEARCH, PRACTICE OR POLICY**

- ⇒ Integrative multiomics enhancer activity profiling may be used to stratify patients with diverse CCA for different tailored targeted therapies, enable identification of new actionable targets, and provide mechanistic insights into cancer development for each identified group.
- ⇒ Our findings may help to accelerate the clinical development of MTOR and oxidative phosphorylation inhibitors for ESTRO and OXPHO group of CCA patients, respectively.
- ⇒ Orthogonal approaches to study tumour microenvironment (NanoString, multiplex immunohistochemistry staining (Vectra) and single-cell spatial transcriptomics (Visium)) allow better understanding of tumour heterogeneity and cellular interaction patterns, which may reveal novel immune targets for treatment and help to improve effectiveness and reduce resistance to immune checkpoint inhibitors for patients with diverse CCA.

Although previous studies have identified molecular alterations associated with distinct CCA subtypes, differences at the level of gene regulation remain largely unexplored, even though this may inform therapeutic strategies. In our previous study, we identified four CCA subtypes which were associated with distinct etiologies, mutations and aberrations in DNA methylation.<sup>4</sup> One subtype (cluster 1 CCA), associated with liver fluke infection, is highly prevalent in Southeast Asian countries such as Thailand and Cambodia, enriched in p53 mutations and exhibits aberrant DNA methylation at CpG islands. One subtype (cluster 4 CCA) is fluke-negative, more commonly found in Western countries, and is associated with mutations in the epigenetic modifier genes such as *BAP1* and *IDH1/2*, with aberrant DNA methylation at CpG shores (regions flanking CpG islands). Another subtype (cluster 3 CCA) is associated with upregulation of immune checkpoint genes.

Several studies have implicated epigenetic aberrations in CCA oncogenesis, subtype identity and disease prognosis.<sup>4 6 7</sup> Despite this, our knowledge of the CCA epigenome is largely limited to aberrant DNA methylation. Enhancers are *cis*-acting regulatory regions distal to gene promoters, and they govern a wide range of cellular processes including cell identity, cell growth

and response to signalling. The dysregulation of enhancers has emerged as a key axis in cancer epigenetics, and their studies in other cancers have uncovered novel oncogenic processes, subtype determinants and putative therapeutic targets.<sup>8–11</sup> Enhancer activities have not been investigated in CCA, despite aberrant DNA hypermethylation and frequent mutations in chromatin modifiers suggesting distinct global enhancer dysregulation in different CCA etiologies. Characterising the CCA enhancer landscape and elucidating the mechanisms underlying enhancer dysregulation can deepen our understanding of CCA tumorigenesis and open up novel therapeutic strategies for CCA.

In this study, we performed integrative analysis of the enhancer and transcriptomic landscape of CCA from different etiologies and found divergent aberrations in enhancer activities. We identified three CCA groups with distinct enhancer profiles and different dysregulated pathways, which were also associated with distinct CCA etiologies: the ESTRO, OXPHO and IMMUN groups. The ESTRO group displayed aberrant activation of the estrogen signalling pathway and was comprised mostly of fluke-positive CCAs. The OXPHO group displayed aberrant activation of the oxidative phosphorylation pathway and was associated with hypermethylated *BAP1* and *IDH*-mutant fluke-negative CCAs. Finally, immune-related pathways were upregulated in the IMMUN group, which was made up of an immunogenic CCA subtype as well as CCA with aristolochic acid (AA) mutational signatures. Spatial transcriptomics revealed intratumoural differences in immune cell populations to be correlated to AA mutation load. Significantly, inhibitors of these pathways were able to attenuate tumour growth in cell lines and mice xenograft models. Therefore, integrative multiomics profiling of enhancer activities may represent a seminal approach to uncover novel therapeutic vulnerabilities in CCA from different etiologies.

**RESULTS****Differential enhancer analysis revealed three distinct CCA enhancer groups tied to different etiologies**

We generated H3K27ac profiles for 63 CCA tissues and 8 normal bile duct tissues (online supplemental figure S1, online supplemental table S1A). After quality checks, the average number of aligned reads was 27.4M per sample. We also generated H3K27ac profiles for 12 CCA cell lines and 1 non-cancer cholangiocyte cell line (19 samples including replicates, online supplemental table S1B), with an average of 17.9M aligned reads per sample. We generated RNA-seq data for 60 CCA tissues, 6 normal tissues and all 13 cell lines (16 samples including replicates). Peak-calling of H3K27ac signals on the tissue samples derived an average of 162.3K peaks called per sample (127.3k enhancer peaks, 34.9k promoter peaks), with 474.1k total consensus enhancers (enhancer peaks present in at least 2 samples) (online supplemental table S1C). We mapped 189.5k consensus enhancers (40.0% of consensus enhancers) to 15.6k genes (81.2% of reference genes) by correlation analysis between enhancer H3K27ac and gene expression, with an average distance of 348.9 kbp from each enhancer to target promoter (online supplemental figure S2A).

Unsupervised clustering of tumour samples derived three CCA enhancer groups with distinct enhancer profiles (figure 1A, online supplemental figure S2B). To check the robustness of these enhancer groups, we performed consensus clustering to repeatedly subsample and cluster the samples. A stable consensus clustering was obtained using  $k=7$  clusters, and samples within each of the three enhancer groups were clustered together almost all the time in the consensus clusters (92.5% on average,

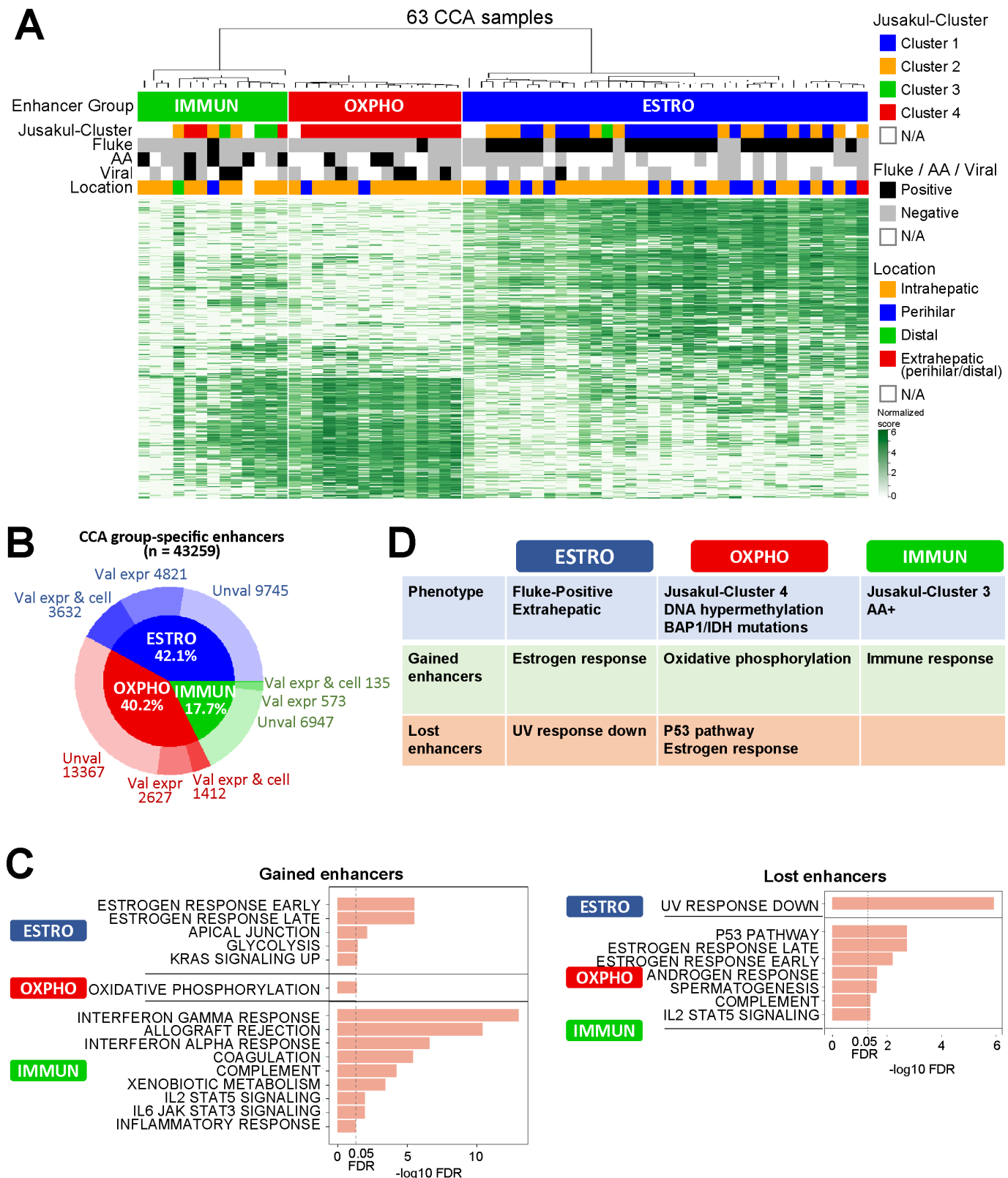


**Figure 1** Differential enhancer analysis revealed varied pathways enriched in CCA from different etiologies (A) Unsupervised clustering of varied CCA tumour samples derived three CCA enhancer groups with distinct enhancer profiles. Heatmap colours represent DiffBind-normalised scores. Jusakul-Cluster refers to the cluster a sample was assigned to in Jusakul *et al.*<sup>4</sup> (B) Pie chart showing the number of somatic-gained group-specific enhancers that were validated (val) or unvalidated (unval) by gene expression and in cell lines for the three groups identified. (C) Distinct enriched pathways identified by Gene Set Enrichment Analysis (GSEA) of validated somatic group-specific enhancers and ranked by FDR. (D) Summary of the pathways unique to each of the three CCA groups. AA, aristolochic acid; CCA, cholangiocarcinoma; FDR, false discovery rate.

online supplemental figure S2C). Consensus clustering split the samples into more clusters than the three enhancer groups (7 vs 3) and revealed that some groups may be further split into smaller subgroups, but these further splits suffered from lower consensus scores. We, therefore, retained the three enhancer groups, which we named the ESTRO, OXPHO and IMMUN enhancer groups for downstream analysis. Notably, the enhancer groups as well as the normal samples could be distinguished in the first two principal components (online supplemental figure S2B).

The ESTRO enhancer group was enriched in fluke-positive samples (27/35 samples, Fisher's test  $p=2.1\times 10^{-8}$ ) but depleted in other risk factors (no AA-positive samples and only one viral-hepatitis-positive sample, Fisher's test  $p=3.09\times 10^{-3}$  and  $p=0.041$  respectively), suggesting that CCA caused by liver fluke infection may be linked to a distinct pattern of enhancer dysregulation. This group was also associated with extrahepatic tumours (peri-hilar or distal, 13/35 samples, Fisher's test  $p=0.047$ ), which is in keeping with previous studies.<sup>4</sup> The OXPHO enhancer group was enriched in cluster 4 CCAs from Jusakul *et al*<sup>4</sup> (which we termed Jusakul-cluster 4 here, 14/15 samples, Fisher's test  $p=2.6\times 10^{-10}$ ), which was previously characterised by DNA hypermethylation at CpG shore regions and associated with mutations in epigenetic modifier genes *IDH1* and *BAP1*.<sup>4</sup> Finally, the IMMUN enhancer group was composed of a more heterogeneous set of samples that clustered outside of the other groups. This group was enriched in Cluster 3 CCAs from Jusakul *et al*<sup>4</sup> (which we termed Jusakul-cluster 3, 3/13 samples, Fisher's test  $p=0.012$ ) and AA-positive CCAs (5/13 samples, Fisher's test  $p=0.035$ ). Notably, the Jusakul-Cluster 3 CCAs were previously characterised by upregulation of immunogenic genes.<sup>4</sup> None of the enhancer groups were significantly enriched with viral hepatitis cases.

We developed an analysis pipeline to derive and validate somatically gained or lost enhancers specific to each CCA enhancer group (online supplemental figure S3). These validated somatically gained group-specific enhancers exhibited gains in the group versus the normal samples and versus the other groups; were accompanied by upregulation in the expression of their associated genes in the group versus the normal samples and versus the other groups; were present in tumour cell lines; and exhibited corresponding gains in the tumour cell lines versus the normal cell lines. The validated somatically lost group-specific enhancers were derived analogously. Among 43 259 somatically gained group-specific enhancers, 5179 were accompanied by gene expression changes and validated in cell lines (12.0%), of which 3632 (70.1%) were ESTRO-specific, 1412 (27.3%) were OXPHO-specific and 135 (2.6%) were IMMUN-specific (figure 1B, online supplemental table S2).

Gene Set Enrichment Analysis (GSEA) of these validated somatic group-specific enhancers revealed distinct enriched pathways (figure 1C, online supplemental table S3). The ESTRO group exhibited gains in estrogen-response genes (Fisher's test false discovery rate (FDR)= $3.0\times 10^{-6}$ ), and losses in genes down-regulated in response to ultraviolet (UV) radiation (Fisher's test FDR= $1.1\times 10^{-6}$ ). The OXPHO group exhibited gains in oxidative phosphorylation genes (GSEA FDR=0.044), and losses in P53 pathway genes (Fisher's test FDR= $1.8\times 10^{-3}$ ) and estrogen response genes (Fisher's test FDR= $1.8\times 10^{-3}$ ). The IMMUN group exhibited gains in immune-response genes such as interferon gamma response genes (Fisher's test FDR= $9.5\times 10^{-14}$ ), interferon alpha response genes (Fisher's test FDR= $2.4\times 10^{-7}$ ), IL2-STAT5 signalling genes (Fisher's test FDR=0.011) and IL6-JAK-STAT3 signalling genes (Fisher's test FDR=0.011), while no enriched pathways were observed among its lost enhancers.

The salient pathways unique to each of the three CCA groups are summarised in figure 1D. These pathways represent potential biomarkers to distinguish between these three groups of CCA and may also point to potentially actionable targets for targeted therapy.

### Estrogen-response enhancers were activated in ESTRO group

The ESTRO enhancer group exhibited somatic gains in 3632 enhancers that were not shared with the other 2 groups, and which were validated by cell-line data and accompanied by increased gene expression (figure 2A). These gained enhancers were enriched in the estrogen-response pathway (387/3632 enhancers, associated with 41 estrogen-response genes, Fisher's test FDR= $3.2\times 10^{-6}$ , figure 2B, online supplemental figure S4A, online supplemental tables S2 and 3).

Interestingly, all three CCA groups exhibited somatic enhancer gains in estrogen-response genes, and a large number of these enhancers were non-group-specific (ie, shared between two or more CCA groups) (figure 2C), suggesting a common dysregulation of estrogen response in CCA in general. However, the ESTRO group gained a large number of estrogen-response enhancers that were specific to that group (36.9% ESTRO-specific enhancers), while the OXPHO and IMMUN groups gained mostly shared estrogen-response enhancers and very few group-specific enhancers (9.2% OXPHO-specific and 1.1% IMMUN-specific enhancers, respectively). This pointed to a unique activation of the estrogen-response pathway in the ESTRO group. Motif analysis of the gained estrogen-response enhancers in the ESTRO group revealed motif enrichment of the Kruppel-like factors (KLF) family of transcription factors, whereas estrogen-receptor motifs were not enriched (online supplemental figure S4B, online supplemental table S2). The most significantly enriched motif belonged to KLF5 (FDR= $2.0\times 10^{-4}$ , Homer) which was present in 53.8% of the gained estrogen-response enhancers. Notably, the KLF5 enhancer was among the validated somatically gained enhancers in the ESTRO group (online supplemental figure S4C). Enhancer activity and gene expression for KLF5 was also significantly higher in the ESTRO group versus each other group (all FDR<0.05, DiffBind, online supplemental figure S4C).

Because estrogen is a master regulator of a large number of genes, initiating the activation of multiple pathways, and is known to crosstalk with other pathways, particularly in CCA,<sup>12–20</sup> we analysed the gained estrogen-response enhancers to see if they were also associated with other pathways. We found that the gained estrogen-response enhancers that were specific to the ESTRO group were most enriched in the PI3K/AKT/MTOR signalling pathway (40/387 estrogen-response enhancers associated with PI3K/AKT/MTOR signalling pathway genes, Fisher's test FDR= $3.7\times 10^{-26}$ ), followed by the P53 pathway (56/387 estrogen-response, Fisher's test FDR= $2.8\times 10^{-20}$ ) and heme metabolism (29/387 estrogen-response enhancers, Fisher's test FDR= $3.4\times 10^{-20}$ ) (figure 2D).

The PI3K/AKT/MTOR and estrogen-signalling pathways are known to crosstalk and interact to activate a common set of estrogen-response genes.<sup>12–21</sup> Consistent with our enhancer and pathway analysis, we found the activity of the activated phosphorylated forms of AKT and MTOR target p70S6 kinase to be higher in fluke-positive compared with fluke-negative cell lines (online supplemental figure S4D), suggesting activated PI3K/AKT/MTOR pathways in fluke-positive cells. We then treated different fluke-positive and fluke-negative CCA cell lines with the MTOR inhibitor rapamycin and observed greater inhibition

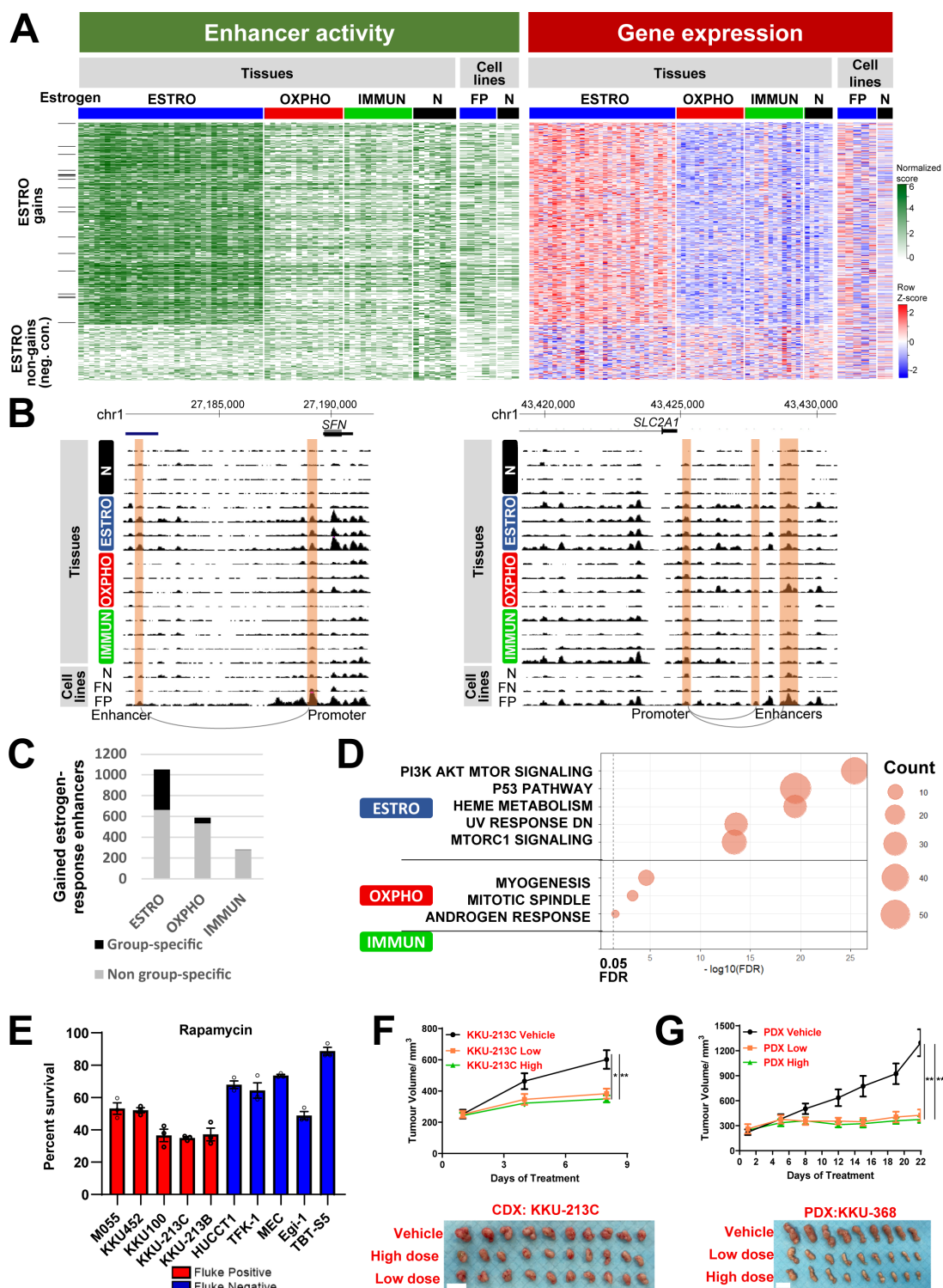


**Figure 2** Enhancers in the estrogen response pathway were gained in the ESTRO group. (A) Heatmap of enhancer activity (left) and gene expression (right) for validated somatically gained enhancers specific to the ESTRO group. Heatmap colours represent DESeq2-normalised scores and DESeq2-normalised row-Z scores. The bottom rows of the heatmap are randomly chosen enhancers not gained in the ESTRO group (negative control for visualisation). (B) H3K27ac signal tracks of two representative estrogen response genes. The positions of the enhancers and promoters are highlighted in orange. (C) Bar chart showing the number of group-specific and non-group-specific gained estrogen-response enhancers in the three CCA groups. (D) Pathways identified by gene set enrichment analysis (GSEA) for gained estrogen-response enhancers specific to each CCA group. (E) Percentage survival of a panel of fluke-positive and fluke-negative CCA cell lines to rapamycin, an MTOR inhibitor. Error bars represent SEM of three biological replicates. (F) Drug study in mouse cell line-derived xenograft models KKU-213C (fluke-positive) showed effectiveness of everolimus. Vehicle=control (n=10), low dose=2.5 mg/kg everolimus (n=10), high dose=5 mg/kg everolimus (n=12). Scale bar represents 2 cm. Error bars represent SEM. (G) Drug study in mouse patient-derived xenograft models KKU-368 (fluke-positive patient derived tumour) showed effectiveness of everolimus compared with vehicle (control). Vehicle=control (n=9), low dose=2.5 mg/kg everolimus (n=9), high dose=5 mg/kg everolimus (n=9). Scale bar represents 2 cm. Error bars represent SEM. \*p<0.05, \*\*p<0.005; calculated using Student's t-test. CCA, cholangiocarcinoma; FN, fluke-negative; FP, fluke-positive; N, normal.

of growth of fluke-positive CCA cell lines compared with fluke-negative cell lines (**figure 2E**, online supplemental figure S4E,F). Similarly, everolimus, a derivative of rapamycin and more potent against mTORC2,<sup>22</sup> was able to effectively inhibit the growth of fluke-positive tumours in cell line-derived mouse xenograft models (**figure 2F**) and fluke-positive patient-derived xenograft models (**figure 2G**). While everolimus was also effective for fluke-negative tumours in cell line-derived mouse xenograft models (online supplemental figure S4G), the percentage tumour suppression (around 30% reduction) was lower as compared with that of fluke-positive tumours in mouse xenograft models (around 50%–70% reduction). Thus, our enhancer profiling analysis and experiments suggest that MTOR inhibitors may be repurposed to inhibit tumour growth clinically for fluke-positive CCAs.

### Enhancers of the oxidative phosphorylation pathway were activated in OXPHO group

The OXPHO enhancer group, associated with *BAP1* loss of function mutations (7/15, Fisher's test  $p=3.2\times 10^{-4}$ ) and *IDH1/2* gain of function mutations (3/15, Fisher's test  $p=0.011$ ), gained 1412 enhancers that were not shared with the other two groups, and which were validated by cell line data and accompanied by increased gene expression (**figure 3A**). These OXPHO-specific gained enhancers were enriched in genes in the oxidative phosphorylation pathway (24/1412 enhancers, associated with seven pathway genes, GSEA FDR=0.044, **figure 3B**, online supplemental figure S5A, online supplemental tables S2 and online supplemental tables S3). The protein levels of the different complexes in the electron transport chain (ETC) regulating mitochondria respiration were also higher in fluke-negative cell lines as compared with fluke-positive cell lines (online supplemental figure S5B). Intriguingly, fluke-negative cell lines have lower basal mitochondrial oxygen consumption rate (OCR) and lower respiratory reserve capacity as accessed by the Seahorse XF Cell Mito Stress Test (**figure 3C**), suggesting reduced mitochondria respiration mediated by oxidative phosphorylation. Fluke-negative cell lines also had decreased mitochondria activity (MitoTracker Red CMXRos staining) as compared with fluke-positive cell lines despite higher total mitochondria levels (MitoTracker Green FM staining) (**figure 3D**). This suggests that the high expression of oxidative phosphorylation genes and proteins of complexes could be a result of feedback regulation stemming from reduced oxidative phosphorylation activities in OXPHO tumours.

IACS-010759 and mubritinib are small molecule inhibitors that inhibit complex I of the ETC, which are in clinical development for acute myeloid leukaemia.<sup>23–25</sup> We showed that fluke-negative tumours were more sensitive than fluke-positive tumours to IACS-010759 (**figure 3E**, online supplemental figure S5C) and Mubritinib (**figure 3F**, online supplemental figure S5D) in *in vitro* cell models. Drug studies in mouse xenograft models also showed better effectiveness of IACS-010759 for fluke-negative tumours compared with fluke-positive tumours (**figure 3G–H**, online supplemental figure S5E–F). Similarly, in fluke-negative PDX model, IACS-010759 remarkably suppressed tumour progression and prolonged the survival of the mice (**figure 3I**). Targeting oxidative phosphorylation was therefore effective for fluke-negative CCAs.

### Immunogenic CCA tumours in IMMUN group

The IMMUN enhancer group, composed of Jusakul-Cluster3 CCAs and AA-positive CCAs, gained 135 enhancers that were

not shared with the other two groups, and which were validated by cell-line data and accompanied by increased gene expression (**figure 4A**). These IMMUN-specific enhancers had a distinct immunogenic profile, and were enriched in immune-response pathways such as interferon gamma response (24/135 enhancers, associated with 18 pathway genes, Fisher's test FDR= $9.5\times 10^{-14}$ ), interferon alpha response (12/135 enhancers, associated with nine pathway genes, Fisher's test FDR= $2.4\times 10^{-7}$ ), IL2-STAT5 signalling (11/135 enhancers, associated with six pathway genes, Fisher's test FDR=0.011) and IL6-JAK-STAT3 signalling (6/135 enhancers, associated with four pathway genes, Fisher's test FDR=0.011) (**figure 4B**, online supplemental figure S6A, online supplemental table S2, online supplemental tables S3).

Because the IMMUN group comprised both Jusakul-Cluster3 CCAs and AA-positive CCAs, we checked if its enriched pathways were also observed when considering these two subgroups alone. Indeed, the IMMUN group's Jusakul-Cluster3 CCAs exhibited gains in interferon gamma response genes (Fisher's test FDR= $1.3\times 10^{-3}$ ) and interferon alpha response genes (Fisher's test FDR= $1.5\times 10^{-3}$ ); while the IMMUN group's AA-positive CCAs exhibited gains in interferon gamma response genes (Fisher's test FDR= $7.0\times 10^{-8}$ ), interferon alpha response genes (Fisher's test FDR=0.031) and IL7-JAK-STAT3 signalling genes (Fisher's test FDR= $2.1\times 10^{-3}$ ) (online supplemental table S2). This demonstrated that the activated immune-response enhancers in the IMMUN group were not restricted to any subgroup within it.

The distinct immunogenic profile of the IMMUN group may reflect immune cell infiltration in these tumour samples. Therefore, we performed NanoString PanCancer IO 360™ Gene Expression Panel to characterise the immune profile of 60 CCA samples (32 ESTRO group, 15 OXPHO group, 13 IMMUN group, and found more gene sets related to immune cell infiltration upregulated in the CCA tumours from the IMMUN group compared with the other groups (**figure 4C**), with enriched gene signatures from antigen presentation (IMMUN vs ESTRO:  $p=0.001653$ , IMMUN vs OXPHO:  $p=0.018493$ ), interferon signalling (IMMUN vs ESTRO:  $p=0.010854$ , IMMUN vs OXPHO:  $p=0.024348$ ) and immune cell migration and adhesion pathways (IMMUN vs ESTRO:  $p=0.001595$ , IMMUN vs OXPHO:  $p=0.041629$  (**figure 4D**)). Surprisingly, the fluke-positive CCAs, where the tumours are known to be in a state of chronic inflammation, were found to have the lowest immune cell infiltration population and immune gene signalling. TNF signalling, which is proinflammatory, was enhanced in fluke-positive CCAs. It has been reported that TNF signalling help cancer cells to evade immune surveillance<sup>26</sup> and could be plausible explanation for the loss of immunogenicity in the fluke-positive CCAs.

We used VECTRA<sup>27–29</sup> to stain selected immune markers on tumour and immune cells to investigate the proportion of tumour infiltrating immune cells in the IMMUN group. We found that immune cells (numbers normalised to CD68+cells) such as cytotoxic T-cells (CD8+) and Treg immune cells (represented by Foxp3+cells) were enriched in the IMMUN group (**figure 4E** and online supplemental figure S6B), which could partially be due to the decrease in PD-L1 and PD-L2, including PD-L1 and PD-L2 in all cells, and proportion of PDL1+CD68+ and PD-LD2+CD68+ immune cells in the IMMUN group. The decreases of PD-L1 and PD-L2 are intriguing because the total CD68+macrophages were higher in the IMMUN group. Overall, these suggest greater tumour infiltrating immune cells in the

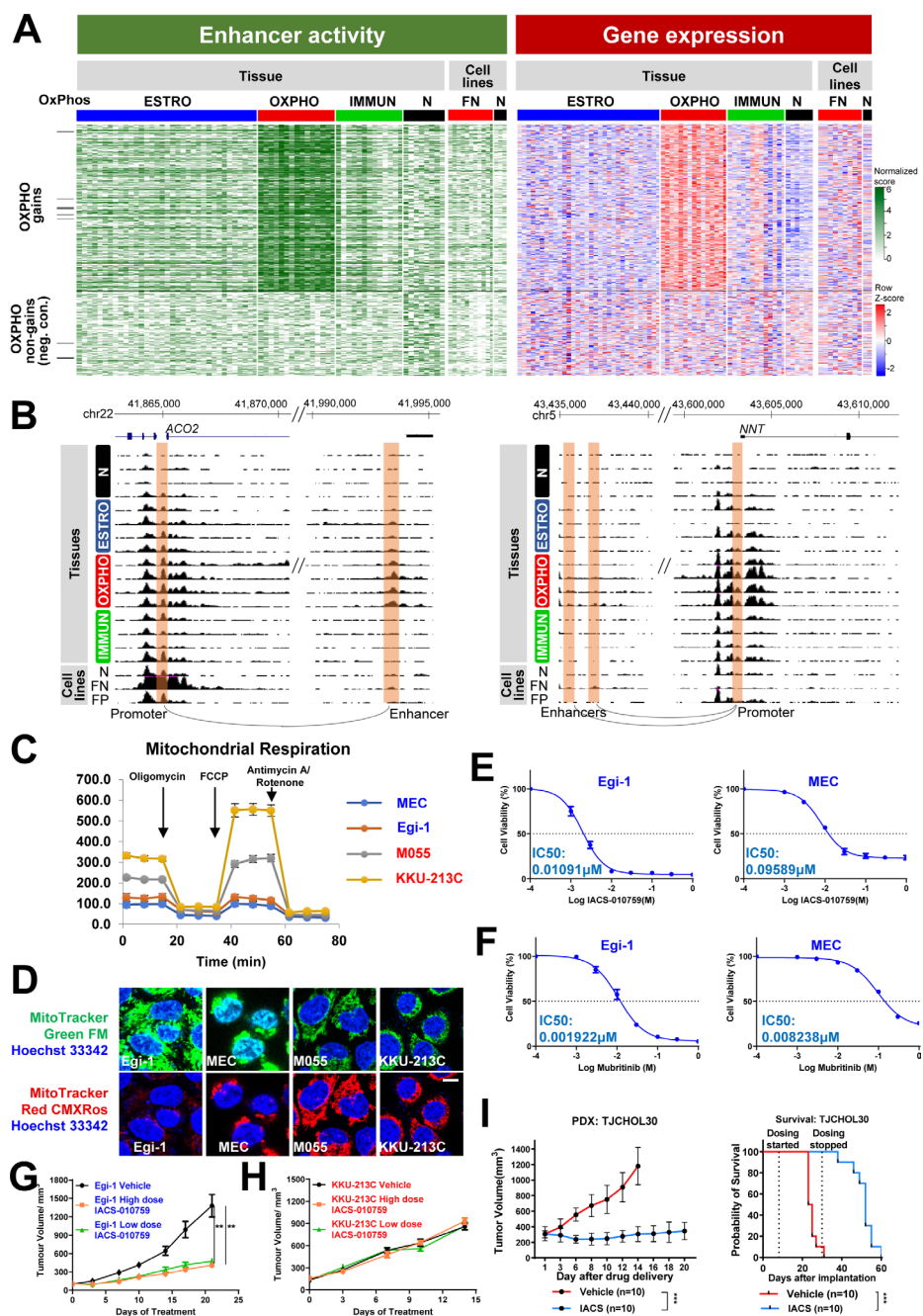


**Figure 3** Enhancers in the oxidative phosphorylation pathway were activated in the OXPHO group (A) Heatmap of enhancer activity (left) and gene expression (right) for validated somatically gained enhancers specific to the OXPHO group. Heatmap colours represent DESeq2-normalised scores and DESeq2-normalised row-Z scores. The bottom rows of the heatmap are randomly chosen enhancers not gained in the OXPHO group (negative control for visualisation). (B) H3K27ac signal tracks of two representative genes regulating oxidative phosphorylation. The positions of the enhancers and promoters are highlighted in orange. (C) Seahorse XF Cell Mito Stress Test showed decreased mitochondria respiration for CCA fluke-negative (in blue font) compared with fluke-positive (in red font) cell lines. Error bars represent SEM. (D) MitoTracker Red CMXRos staining also showed decreased mitochondria activity for CCA fluke-negative compared with fluke-positive cell lines, while MitoTracker Green FM staining showed high total mitochondria levels for CCA fluke-negative compared with fluke-positive cell lines. Scale bar represents 20 µm (E) Drug-dose response curves for IC<sub>50</sub> showed that fluke-negative cell lines were sensitive to IACS-010759. Error bars represent SEM of three biological replicates. (F) Drug-dose response curves for IC<sub>50</sub> showed that fluke-negative cell lines were sensitive to Mubritinib. Error bars represent SEM of three biological replicates. (G) Drug study in cell line-derived mouse xenograft models Egi-1 (fluke-negative) revealed that IACS-010759 was effective for fluke-negative tumours. Vehicle=control (n=8), low dose=1 mg/kg IACS-010759 (n=10), high dose=5 mg/kg IACS-010759 (n=10). Error bars represent SEM. (H) Drug study in cell line-derived mouse xenograft models KKU-213C (fluke-positive), which was not effective, revealed that IACS-010759 was more effective for fluke-negative tumours compared to fluke-positive tumours. Vehicle=control (n=20), low dose=1 mg/kg IACS-010759 (n=22), high dose=5 mg/kg IACS-010759 (n=20). Error bars represent SEM. (I) Drug study in fluke-negative CCA patient-derived xenograft model TJCHOL30 showed that IACS-010759 suppressed tumour growth and prolonged survival of the mice compared with control. Vehicle=control (n=10), IASC=1 mg/kg IACS-010759, (n=10). Error bars represent SEM. \*\*p<0.005; \*\*\*p<0.0005 calculated using Student's t-test. CCA, cholangiocarcinoma; FN, fluke-negative; FP, fluke-positive; IASC, IASC-010759; N, normal.

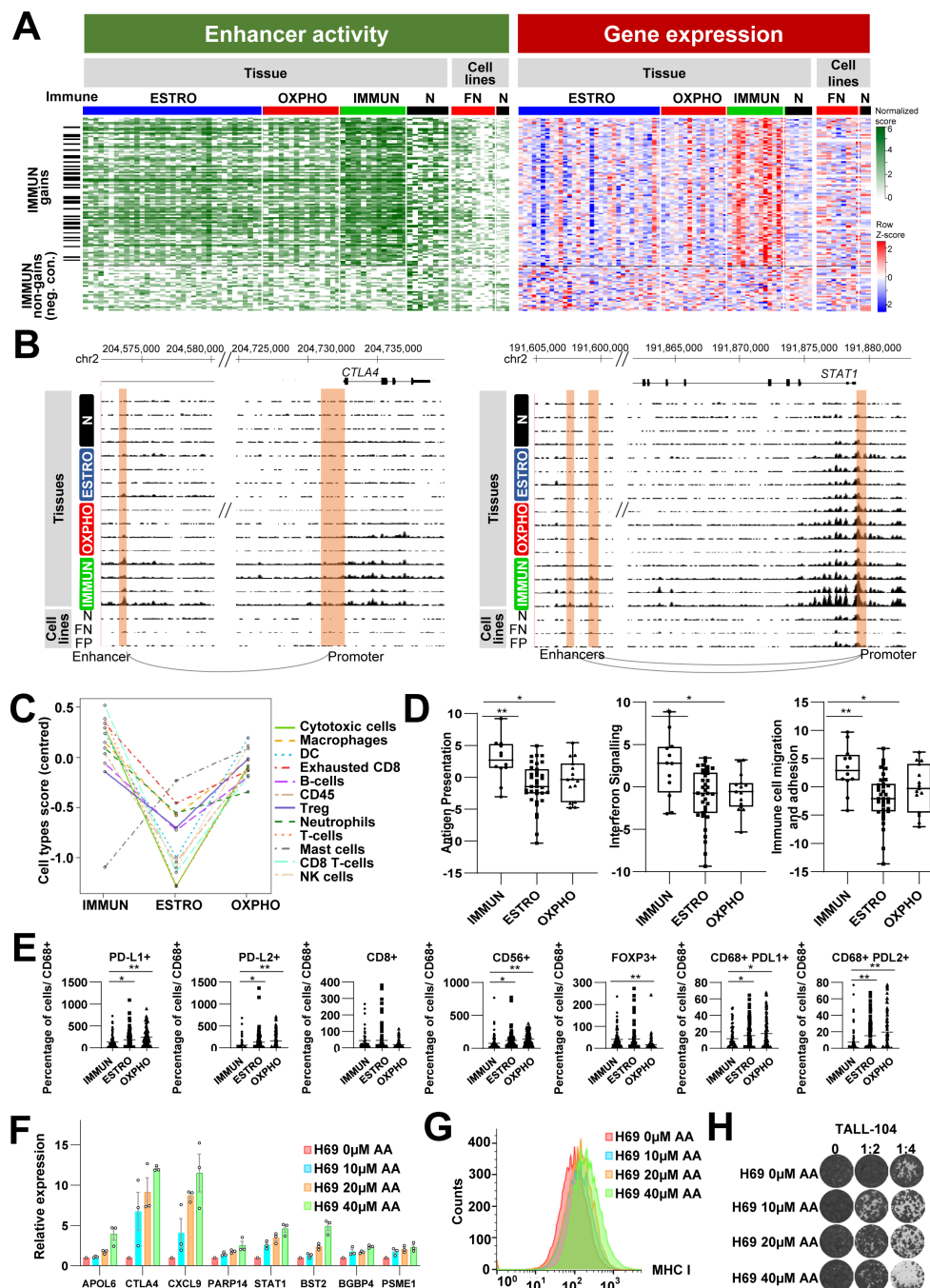


**Figure 4** Immune-related enhancers were upregulated in the IMMUN group (A) Heatmap of enhancer activity (left) and gene expression (right) for validated somatically gained enhancers specific to the IMMUN group. Heatmap colours represent DESeq2-normalised scores and DESeq2-normalised row-Z scores. The bottom rows of the heatmap are randomly chosen enhancers not gained in the IMMUN group (negative control for visualisation). (B) H3K27ac signal tracks of two representative genes of immune response pathways. The positions of the enhancers and promoters are highlighted in orange. (C) NanoString PanCancer IO 360™ Gene Expression Panel to characterise the immune profile of 60 CCA samples (32 ESTRO group, 15 OXPHO group, 13 IMMUN group) revealed more immune cell infiltration in the CCA tumours from the IMMUN group compared with the ESTRO and OXPHO groups. (D) Gene signatures from antigen presentation, interferon signalling and immune cell migration and adhesion pathways were enriched in the IMMUN group compared with other CCA clusters. The scores from each gene signature of each sample are represented in a boxplot. (E) Quantification of indicated immune cells in indicated cluster with positive IHC staining using VECTRA, normalised to the number of CD68+ stained cells for each image. Each dot represents one region of interest imaged. A total of 97 ROIs are from IMMUN cluster, 101 ROIs are from ESTRO cluster and 104 ROIs are from OXPHO cluster, representing 10 tumours from IMMUN cluster and 11 tumours each from ESTRO and OXPHO cluster. The data are represented in a dotplot. Horizontal bar represents mean. (F) qPCR showing the expression of the indicated genes in H69 (normal bile duct cell line) treated with the indicated dose of AA as compared with non-treated H69 for 180 days. Error bars represent SEM of three biological replicates. (G) Flow cytometry showing dose-dependent increased cell surface MHC-I levels in H69 cells treated with the indicated dose of AA for 180 days. (H) H69 cells treated with the indicated dose of AA for 180 days were co-cultured with immortalised cytotoxic T-cells TALL-104 in the indicated ratio for 9 days. The H69 cells were then stained with crystal violet staining to show the susceptibility to TALL-104 cells. \* $p<0.05$ , \*\* $p<0.005$ ; calculated using Student's t-test. AA, aristolochic acid; CCA, cholangiocarcinoma; FN, fluke-negative; FP, fluke-positive; N, normal.

IMMUN group, which could be due to attenuated immune inhibitory signals.

AA is a natural compound found in many plants of the *Aristolochia* genus. *Aristolochia* plants are used in traditional herbal remedies for weight loss, menstrual symptoms and rheumatism. Consumption of AA is a known cause of intrahepatic CCA.<sup>30</sup> Normal bile duct cells were incubated with different doses of AA for 180 days and allowed to recover from treatment for at least 1 month. The level of AA-specific mutation signature 22 increased in treated cells in an AA dose dependent manner (online supplemental figure S6C), and therefore, the treated cells were representative of CCA tumours with AA signatures. It was found that the same set of genes that were upregulated in the IMMUN group was also enhanced in AA treated cells in a dose-dependent manner (online supplemental figure S6A and figure 4F). Antigen presentation represented by cell-surface MHC class I levels was increased in AA treated cells (figure 4G) and AA treated cells were consequentially less tumourigenic when co-cultured with cytotoxic T-cell TALL-104 (figure 4H, online supplemental figure S6D). Taken together with NanoString and VECTRA results, our data suggest that tumours from the IMMUN group are more immunogenic and amenable to immunotherapy.

To further investigate the relationship between AA-specific mutation signature and immune response, we performed Visium Spatial Gene Expression analysis on 4 CCA tissues: TW\_33 (AA-positive with AA mutation count at 42500, IMMUN group), Z2403 (AA-negative, IMMUN group), A157 (ESTRO group) and Z2778 (OXPHO group) (figure 5A). BayesSpace ( $k=4$ )<sup>31</sup> was used to cluster the Visium transcriptomics dataset into four clusters in each tissue, and then MCP-counter<sup>32</sup> was applied to determine the immune cell repertoire for each cluster (figure 5A). Consistent with our NanoString and VECTRA analysis, the different immune cell populations were more enriched in each BayesSpace cluster for CCA tissues from IMMUN group compared with from ESTRO and OXPHO group (figure 5A). Using VarTrix (10x genomics) and somatic mutation data from bulk whole genome sequencing data, mutational signature analysis was performed on the Visium dataset for TW\_33 (AA-positive, IMMUN group). All 4 BayesSpace clusters of TW\_33 showed AA-specific mutation signature 22, with clusters 3 and 4 having a higher AA-specific mutation signature load compared with clusters 1 and 2 (online supplemental figure S7 and figure 5B). This suggests that the AA-specific mutation signature load in CCA tissue was heterogeneous. Using CITE-seq human peripheral blood mononuclear cells (PBMC) data<sup>33 34</sup> as a reference, the expressions of the immune markers CD274, CD8, CD68, CD3, CD19 and CD4 were identified, and mapped out in the tissue section of TW\_33 and compared with AA-specific mutation signature (A>T) distribution (figure 5B). Cells with high A>T mutations were negatively correlated with cells with CD274 signature and CD4+T cells, and positively correlated with CD8+T cells, CD3+T cells and CD19+B cells, while no correlation with CD68+ macrophages was observed (figure 5B). Our data suggest that despite the higher immune signatures in CCA tissues from IMMUN, intratumour differences in immune cell repertoire, signalling and responses existed, and in the case of AA-CCA tissues, were correlated to AA mutation load.

## DNA methylation in CCA implicated divergent enhancer activities

DNA methylation is a mechanism for transcriptional repression associated with stable, quasi-permanent repression of genomic regions, and is also linked to enhancer dysregulation.<sup>35</sup> We profiled the DNA methylation of our samples and checked the association between somatic enhancers and the methylation status of CpGs within those enhancers. In both the ESTRO and OXPHO enhancer groups, gained enhancers were associated with DNA hypomethylation ( $401/3733=10.7\%$  and  $37/2661=1.4\%$  of gained enhancers respectively, Fisher's test  $p=2.2\times 10^{-16}$  and  $3.2\times 10^{-9}$ , respectively, figure 6A), suggesting that in these groups, a small portion of enhancers was aberrantly gained in regions previously repressed by DNA methylation. In contrast, no such association was found in the IMMUN group (Fisher's test  $p=0.98$ ).

We checked if lost enhancers were associated with DNA hypermethylation and found that only in the ESTRO group was there a trend of lost enhancers accompanied by DNA hypermethylation ( $23/149=15.4\%$  of lost enhancers, Fisher's test  $p=0.12$ , figure 6B), which was absent in the other groups (Fisher's test  $p=0.99$  and  $0.67$  in the OXPHO and IMMUN groups, respectively, figure 6B). This suggests that lost enhancers that become permanently silenced by DNA methylation were relatively rare and may be confined to the ESTRO group.

To further investigate the divergence in DNA methylation vis-à-vis enhancer dysregulation, we analysed the DNA methylation profiles in an additional 87 CCA samples (giving a total of 150 samples). Since this new superset included many samples without enhancer profiling, we performed clustering based on only the DNA methylation data (figure 6C). We obtained four methylation clusters, which were similar to the methylation clusters obtained in our previous study.<sup>4</sup> Two clusters exhibited DNA hypermethylation. The Blue Methylation Cluster (similar to Jusakul-cluster 1) was hypermethylated within CpG-islands and was enriched in Fluke-positive samples, and among its samples with enhancer profiles (18/35 samples), consisted fully of ESTRO enhancer group samples ( $18/18=100\%$ , Fisher's test  $p=2.0\times 10^{-6}$ ). The Red Methylation Cluster (similar to Jusakul-cluster 4) was hypermethylated in CpG-shore regions and was enriched in tumours exhibiting *IDH1* and *BAP1* mutations, and among its samples with enhancer profiles (15/42 samples), consisted primarily of OXPHO enhancer group samples ( $12/15=80\%$ , Fisher's test  $p=6.5\times 10^{-8}$ ). Notably, we also observed divergence between methylation clusters and enhancer clusters; for example, both the ESTRO and IMMUN enhancer-group samples were split between different methylation clusters. This demonstrates the utility of interrogating both DNA methylation and enhancer profiles, as they provided orthogonal information representing distinct but interacting epigenetic mechanisms.

To further probe the hypermethylation of lost enhancers in the ESTRO group, we investigated the two hypermethylated clusters (the fluke-positive Blue cluster and the *IDH/BAP1*-associated Red cluster) in the 150 samples, and observed that the Blue cluster had a preponderance of hypermethylation within CpG islands versus shore regions ( $481/1381=34.8\%$  hypermethylated within islands vs  $181/1381=13.1\%$  hypermethylated at CpG shores, the remainder being hypermethylated in both islands and shores), while the opposite was true for the Red cluster ( $281/1755=16.0\%$  hypermethylated within islands vs  $472/1755=26.9\%$  hypermethylated at shores). In our previous study, we had proposed that island versus shore methylation

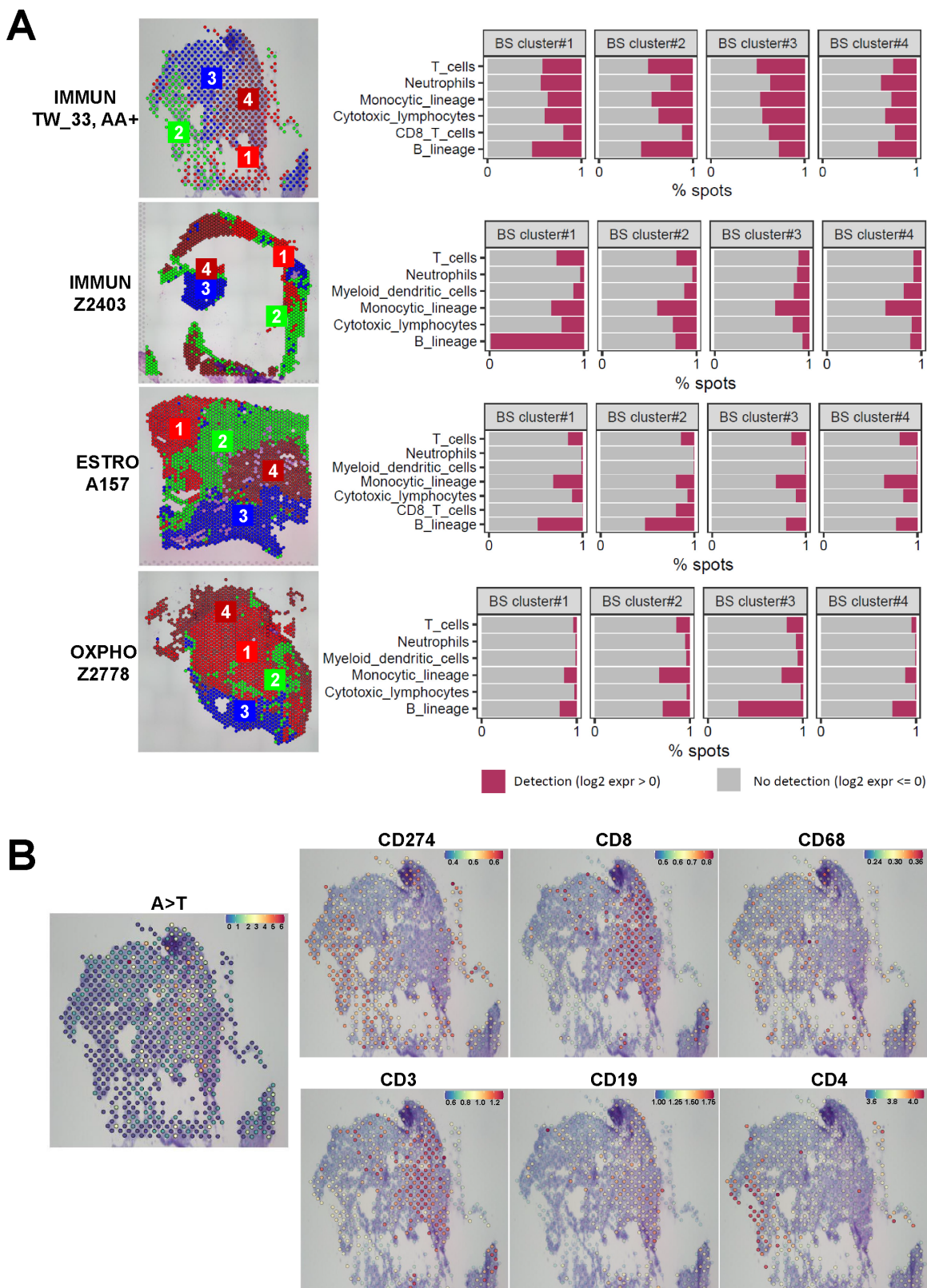


**Figure 5** Correlation of AA mutation signatures load with immune cell distribution identified using spatial transcriptomics (A) Visium Spatial Gene Expression was performed on TW\_33 (AA-positive, IMMUN group), Z2403 (AA-negative, IMMUN group), A157 (ESTRO group) and Z2778 (OXPHO group). Through BayesSpace clustering ( $k=4$ ), the spatial transcriptomics data were grouped into four clusters. The indicated immune cell populations for each cluster were identified using MCP-counter. The expression of the indicated immune cell population from the Visium spots in each cluster (BS cluster #1 to BS cluster #4) is plotted in a bar chart. (B) Cells with A>T mutation signature were spatially identified in TW\_33 (AA-positive, IMMUN group) using VarTrix and somatic mutation data from bulk whole genome sequencing data. The position of immune markers CD274, CD8, CD68, CD3, CD19 and CD4 were mapped out in the tissue section of TW\_33 using CITE-seq PBMC data as reference. AA, aristolochic acid; BS cluster, BayesSpace cluster.

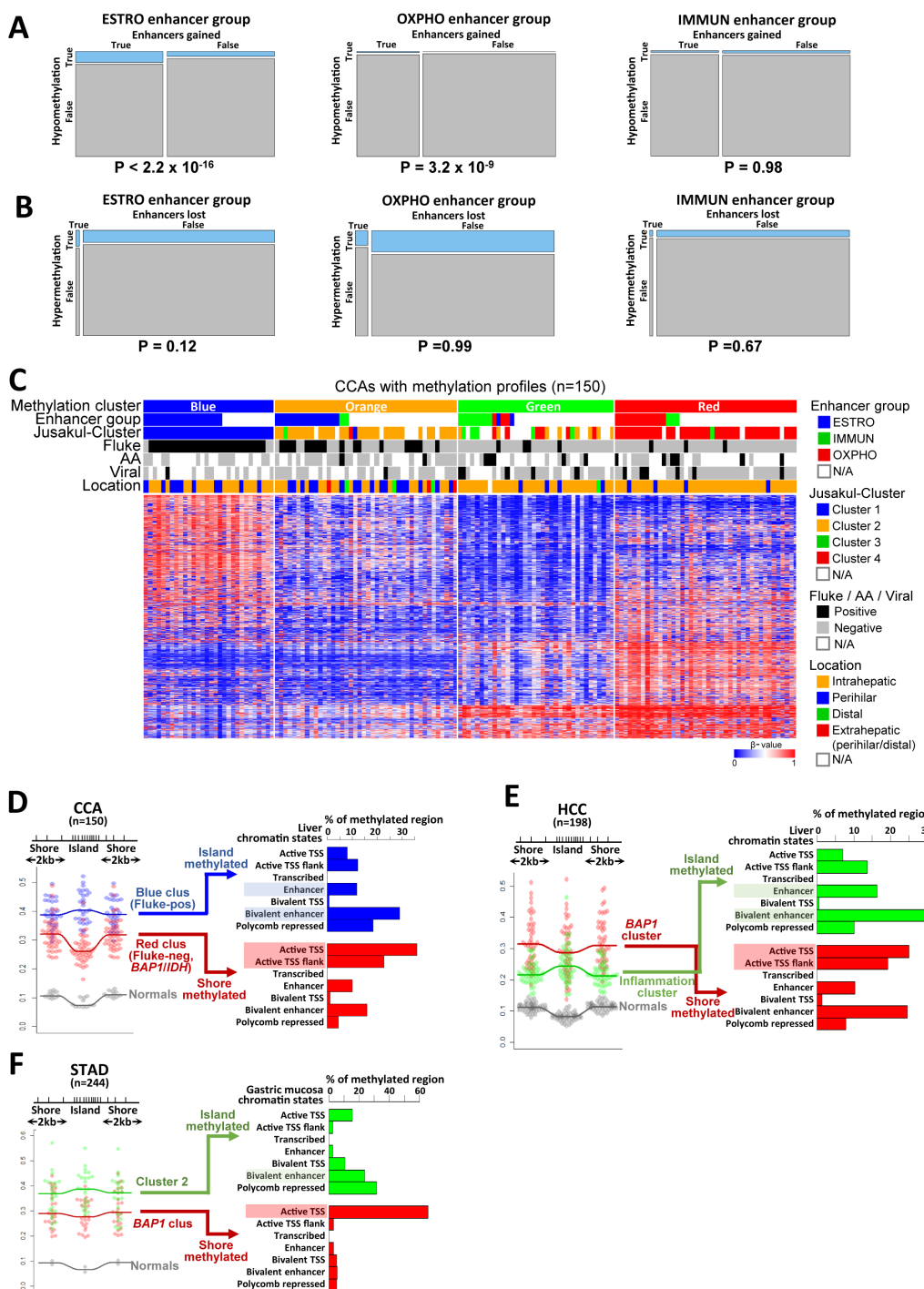


**Figure 6** DNA methylation in CCA implicated divergent enhancer activities (A) Correlation between enhancer gain and DNA hypomethylation. Box heights reflect the proportions of hypomethylated or not-hypomethylated enhancers, while box widths reflect the proportions of gained or not-gained enhancers. Enhancer gain was associated with DNA hypomethylation in the ESTRO and OXPHO groups. P values calculated using Fisher's test. (B) Correlation between enhancer loss and DNA hypermethylation. Box heights reflect the proportions of hypermethylated or not-hypermethylated enhancers, while box widths reflect the proportions of lost or not-lost enhancers. Enhancer loss was not associated with hypermethylation in all groups, but showed a slight trend in the ESTRO group. P values calculated using Fisher's test. (C) Unsupervised clustering of DNA methylation profiles in 150 CCA samples yielded hypermethylated clusters associated with enhancer groups. Heatmap colours represent  $\beta$ -values. (D) Blue and red clusters exhibited distinct hypermethylation patterns within the CpG island/shore topology (left), impacting genomic regions with distinct chromatin states (right). Each dot represents a single sample's mean methylation value ( $\beta$ -value) in the CpG island/shore topology, among its hypermethylated CpG islands. The blue cluster exhibited CpG island methylation enriched in enhancer regions, while the red cluster exhibited CpG shore methylation enriched in active promoter regions. (E) and (F) Analysis of publicly available hepatocellular carcinoma (HCC) and stomach adenocarcinoma (STAD) data revealed similar hypermethylated clusters with distinct hypermethylation patterns within the CpG island/shore topology, impacting genomic regions with distinct chromatin states. In both cancers, a hypermethylated cluster (associated with inflammation in HCC) exhibited CpG island methylation enriched in enhancer regions; while another hypermethylated cluster (associated with BAP1 mutations) exhibited CpG shore methylation enriched in active promoter regions. AA, aristolochic acid; CCA, cholangiocarcinoma; HCC, hepatocellular carcinoma; STAD, stomach adenocarcinoma.

reflected different disease etiologies, with long-standing inflammation associated with fluke infection leading to an accumulation of hypermethylation within CpG islands, while mutations in epigenetic-regulatory genes led to a fast-acting hypermethylation confined to CpG shores.<sup>4</sup> To further investigate this, we mapped aberrant DNA methylation to genome-wide chromatin states in liver tissue from the Roadmap Epigenomics Consortium<sup>36</sup> (bile duct tissue data was unavailable), and found that the Blue cluster exhibited CpG island methylation enriched in enhancer regions, while the Red cluster exhibited CpG shore methylation enriched in active promoter regions (figure 6D). This suggests that some enhancers lost in fluke-positive CCAs were accompanied by DNA hypermethylation which was associated with permanent transcriptional repression. This is consistent with our finding above (figure 6B) that enhancers lost in the ESTRO enhancer group may show a slight association with hypermethylated CpGs.

To corroborate our observations of divergent enhancer-region methylation in CCA, we analysed other cancer types using publicly available DNA methylation, mutation, inferred immune features, and chromatin states data.<sup>36–39</sup> We considered digestive tract organs with inflammation-associated etiologies as well as *IDH/BAP1* mutations (similar to cluster 4 of CCA) and focused on hepatocellular carcinoma (HCC) and stomach adenocarcinoma (STAD). In each cancer, we focused on methylated clusters analogous to the CCA Blue and Red hypermethylated clusters, that is, island-methylated *IDH/BAP1*-wildtype cluster, and shore-methylated *IDH/BAP1*-mutant cluster. Similar to the CCA Blue cluster, the HCC island-methylated cluster was enriched in adjacent tissue inflammation (Fisher's test  $p < 0.05$ ), and both HCC and STAD island-methylated clusters targeted enhancer regions for methylation (figure 6E,F). Moreover, similar to the CCA Red cluster, the shore-methylated clusters in both HCC and STAD were enriched for *IDH/BAP1* mutations (Fisher's test  $p < 0.001$ ,  $p < 0.05$ , respectively), and both targeted promoters for methylation (figure 6E,F). Thus, the associations observed in CCA between disease etiology, methylation topology, and chromatin-state methylation targets were largely recapitulated in HCC and STAD, suggesting that CpG hypermethylation in enhancer dysregulation may be similarly divergent between subtypes in these cancers.

## DISCUSSION

In our previous work, we identified distinct genetic alterations in fluke-positive and fluke-negative CCA tumours.<sup>4 6 40</sup> Subsequently, we also discovered two groups of CCA with distinct DNA hypermethylation topologies: (1) CpG island hypermethylated group characterised by liver fluke infection, *EZH2* and *TP53* mutations, and (2) CpG shore hypermethylated group characterised by *IDH1* and *BAP1* mutations. Over the years, other groups have also genetically, transcriptionally, translationally and post-translationally analysed diverse CCAs of different populations, using multiple biological materials ranging from primary cancer tissues to cancer cfDNA, performing myriad of bulk or single-cell analysis, and investigating various pathways from oncogenic signalling to immune signalling.<sup>4 6 7 40–51</sup> Unfortunately, despite these intensive efforts to improve the characterisation of CCA, therapeutic options are still limited. So far, FDA approval of drugs are only for CCA with *IDH1* mutations or *FGFR*-fusions,<sup>1–3</sup> which make up an approximate merely 20% of global fluke-negative CCA cases. CCA continues to remain an aggressive cancer with poor prognosis and high mortality in both Western countries and Southeast Asia. Events contributing

towards accumulation of genetic, epigenetic and transcriptional alterations are commonplace in CCA. Therefore, an integrative approach to characterise such multidimensional changes is required to better comprehend diverse CCA, and in the process, allowing better understanding of underlying oncogenic mechanisms in different etiologies and unveiling potential etiology-based therapeutic approaches.

To this end, in this study, we seek to decipher genetic and epigenetic changes through integrative multiomics analysis of enhancer analysis and transcriptomic landscapes, and thereafter correlate to the DNA methylation groups<sup>4</sup> which we had previously discovered. Characterising enhancer activity in diverse CCA is currently an uncharted territory. We uncovered 3 groups of CCA tumours using this method: (1) a fluke-positive group with upregulated estrogen signalling (ESTRO), (2) a fluke-negative group with increased expression of genes in the oxidative phosphorylation pathway (OXPHO) and (3) a group made up of highly immunogenic tumours, including those with AA mutational signature (IMMUN). We also found that DNA methylation and enhancer activities were closely associated but not entirely causally dependent on each other, again highlighting the importance of integrative multiomics study. Our study revealed contrasting etiologies of diverse CCA tumours, strongly positing that the same disease manifestation can be in fact driven by vastly different molecular circuitries and that each patient should be treated with appropriately targeted therapy, by using epigenetics modifications as biomarkers of therapy response.

Based on our integrative analysis, we found that specific estrogen-response enhancers were activated in the ESTRO group and motif analysis revealed enrichment of motifs belonging to KLF family of transcription factors, in particular KLF5. Our results show that the enhancer activity and gene transcription of *KLF5* were upregulated in ESTRO group. Evidence suggests that KLF5 is a mediator of both estrogen and PI3K/AKT/MTOR signalling. Estrogen and other steroid hormones have been shown to affect the expression levels of KLF5, and through KLF5 and Er $\beta$ , the angiogenesis and growth of prostate cancers have been found to be affected.<sup>52–54</sup> High levels of KLF5 have been reported to activate the PI3K/AKT/MTOR signalling pathway in melanoma cells to inhibit autophagy<sup>55</sup> and promote hypoxia-induced cell survival and block cell apoptosis in non-small cell lung cancer.<sup>56</sup> Notably, several articles describe the crosstalk between the estrogen signalling pathway and MTOR pathway where the former activates the latter.<sup>12 21 57</sup> Both factors, the high levels of KLF5 and activated estrogen signalling in tumours from the ESTRO group, likely contributed to the upregulated PI3K/AKT/MTOR signalling pathway. It has been reported that MTOR inhibitors may be effective for CCA, but neither the effectiveness in different CCA subtypes nor biomarkers to justify the use have been investigated.<sup>58–62</sup> In this study, we further showed that MTOR inhibitor rapamycin and everolimus more effectively inhibited the growth of fluke-positive CCA over fluke-negative CCA, particularly in patients with activated estrogen and PI3K/MTOR signalling, allowing patient stratification based on etiology and targeted approach, paving the way for the use of other rapalogs or newly discovered drugs to better improve clinical outcomes for these group of patients.

Interestingly, the OXPHO group gained enhancers enriched in genes from the oxidative phosphorylation pathway, as a response to lower mitochondria respiration in the cells. Cells with lower oxidation phosphorylation activity and low spare respiratory capacity in the ETC chain are metabolically vulnerable. Cancers with downregulated oxidative phosphorylation are also typically metastatic and invasive, and prognoses are poor.<sup>63</sup> Acute myeloid

leukaemia cells which have similar low spare respiratory capacity are known to be more susceptible to inhibition of the activity of protein complexes in the ETC.<sup>64</sup> *IDH* mutations have been associated with enhanced mitochondrial oxidative metabolism, and the mechanism for this has been studied in acute myeloid leukaemia,<sup>65</sup> but not in CCA. The OXPHO group was enriched with *IDH* mutants (Fisher's test  $p=0.011$ ), but this constituted only 3/15 patients in this group. Therefore, it may be worth investigating what *IDH*-independent mechanisms may also lead to the same oxidative phosphorylation dysregulation in the group. We demonstrated that fluke-negative tumours were more sensitive to oxidative phosphorylation inhibitor drug IACS-010759 using *in vitro* and *in vivo* models. Even though we did not observe any adverse effects in mice fed with IACS-010759, a recent publication indicates that IACS-010759 may cause unexpected and unwanted side effects such as neurotoxicity in human clinical trials.<sup>66</sup> Nonetheless, our study has shown that oxidative phosphorylation signature is a potential biomarker for effectiveness of oxidative phosphorylation inhibitors, prompting need for further mechanistic studies and development of safe metabolic drugs. In addition, identification of other biomarkers to discover therapeutic drugs that can synergise with IACS-010759, may help to reduce the dosage of IACS-010759 used to clinically safe levels,<sup>67 68</sup> allowing these patients to benefit from the use of metabolic inhibitor drugs. Of significance, the OXPHO enhancer group was primarily composed of fluke-negative cluster 4 CCAs in Jusakul *et al*<sup>4</sup>. These CCAs were characterised by *IDH1/2* gain of function mutations and *BAP1* loss of function mutations, and these could be potential biomarkers for use of another targeted drug in combination with oxidative phosphorylation inhibitors. Even though FDA approved monotherapy are now available for CCA with *IDH1/2* gain of function mutation and *FGFR* alterations, acquired resistance is a common problem<sup>69</sup> and our study may provide a new combination therapeutic strategy for these patients.

In the IMMUN group, there were 38% of the CCA tumours with AA mutation signature. AA is a known group I human carcinogen. Epidemiological study has showed that AA is associated with increasing risk of upper tract urothelial carcinoma in Taiwan.<sup>70–72</sup> Recently, CCAs with AA signatures have also been found in CCA cohorts from diverse populations.<sup>4 30 41 42 44</sup> AA-linked cancer is a major public health issue in many regions such as Taiwan. Through animal studies, AA has been shown to cause intrahepatic CCA.<sup>30</sup> Interestingly, our spatial transcriptomics results elucidate that in CCA tumours with AA mutation signature, intratumour differences in immune signature were present and dependent on the heterogenous intratumour AA mutation signature load, which may affect immunotherapy responses. In addition, AA mutation signature was heterogeneous in the CCA tissues, suggesting that cancers with AA mutation signature may not have arisen from a single lineage. Other than AA-related CCA, the IMMUN group was also made up of tumours with elevated levels of chromosomal aberrations, and high expression of immune checkpoint genes and pathways related to immune signalling through unknown mechanisms. We now show through this study that increased enhancer activity may be one of the factors that contribute to the immune hot nature for this group of tumours. Our results also show that the immune environment of the IMMUN group had more activated immune cells, suggesting the potential of using immunotherapy for this group of CCA tumours. In a recent combination immunotherapy study, only 23% of patients with advanced CCA had objective response.<sup>73</sup> Our study may help to better stratify such patients with CCA for immune checkpoint therapies.

Integrative multiomics profiling is not without limitations. Alterations such as epigenomic changes are dynamic and may be greatly influenced by chronic carcinogenic exposures or environmental factors. Other than fluke infection, CCA is also increasingly associated with primary sclerosing cholangitis and metabolic diseases such as non-alcoholic fatty liver disease, nonalcoholic steatohepatitis, dyslipidaemia, diabetes, metabolic syndrome and obesity.<sup>74–78</sup> These diseases are also characterised by chronic inflammation like fluke infection, and thus widespread aberrant gene mutations, transcriptomics, DNA methylation and enhancer dysregulation are expected. Therefore, a large sample number of tumours from diverse global populations may be required to pinpoint epigenetic aberrations specific to different etiologies of tumour.

Even though our results can be validated *in vitro* and *in vivo*, the conclusions derived should be cautiously examined and further validated. Notably, CCA is characterised by a strong desmoplastic tumour microenvironment. The desmoplastic stroma, also found in other cancers such as lung, colon and breast cancers, is heterogeneous and made up mainly of cancer associated fibroblasts (CAF) and immune cells such as tumour-associated regulatory T lymphocytes (Tregs), macrophages, neutrophils and natural killer cells.<sup>79 80</sup> The CAFs contains fibroblasts and myofibroblast-like cells that influence cancer progression and drug resistance and have also been shown to promote resistance to clinical treatments such as chemotherapeutic drugs, immunochemotherapeutic drugs, and targeted drugs like erlotinib and everolimus.<sup>81–85</sup> These suggest that more complex mouse models, such as early passage PDX models, CCA genetic mouse models and introducing a mix of both cancer cells and CAFs into mice<sup>86 87</sup> are required to better recapitulate the complexity of CCA and drug response. In individual patients, integrative multiomics enhancer profiling and other clinical tests may be required before administration of drug inhibitors. Despite the limitations, the paucity of effective treatments for the vast majority of CCA patients accentuate the urgency for multiomics profiling studies. We heed the call by performing integrative transcriptomic, epigenetic profiling of enhancers activities and DNA methylation profiling, and in the process uncovered new biomarkers and therapeutic approaches, which have advanced the scientific field for CCA and may tackle unmet clinical needs in CCA.

## METHODS

### CCA tumours

Primary tumours and normal samples were obtained from the SingHealth Tissue Repository (Singapore), Khon Kaen University (Thailand), Linkou Chang Gung Memorial Hospital (Taiwan) and Fundeni Clinical Institute (Romania). A summary and list of clinical data is included in online supplemental table S1.

### Cell lines

MEC (Riken), HUCCT1 (HSRRB), TFK-1 (DSMZ) and MEC (Riken) were cultured in RPMI (Gibco)+10% FBS, M055 (JCRB), KKU452 (JCRB) and KKU100 (JCRB) was cultured in Ham's F12 (Gibco)+10% FBS, and Egi-1 (DSMZ), KKU-213B and KKU-213C<sup>88</sup> were cultured in DMEM (Gibco)+10% FBS. TALL-104 (CRL-11386) was cultured in RPMI+20% FBS, supplemented with 5 µg/mL IL-2 (Miltenyi, 130-097744). H69 was obtained from D. Jefferson (New England Medical Center, Tufts University) and cultured in H69 enriched media.<sup>89</sup> TBT-S5 is an in-house derived patient cell line cultured in H69 enriched media. Cell lines were routinely checked to ensure that they

were mycoplasma free and grown in an incubator with 37°C and 5% CO<sub>2</sub>. Early passage number cells (less than 10 passages) were used in experiments.

### RNA-Seq

RNA was extracted using the Qiagen RNeasy Mini kit. Illumina Tru-Seq Stranded Total RNA kit (Illumina, San Diego, California, USA) was used to prepare RNA libraries from 1 µg of total RNA. Paired-end 150 bp sequencing was performed using Illumina HiSeq4000 sequencer with the paired-end 150 bp read option.

### RNA-Seq data processing

We used STAR to align RNA-Seq reads. The reference genome was built from the GRCh37.p13 human genome and RefSeq curated annotations. Mapping quality was checked using Picard-Metrics. Gene count matrices were generated using RSEM. We excluded problematic transcripts (blacklisted transcripts) such as rRNA, snoRNA and MT genes. Differential expression testing was performed using DESeq2. Run-time commands and parameters are provided in the included scripts.

### Nano ChIP-Seq

Nano-ChIP-Seq was performed as previously described.<sup>11–90</sup> Roughly 5 mg of tissues were cross-linked with 1% formaldehyde for 10 min at room temperature and stopped by adding glycine to 0.2M. The tissues were then lysed in lysis buffer and sonicated for lysed in 100 µL lysis buffer and sonicated for 16 cycles (high settings, 30 s on, 30 s off) using a Bioruptor (Diagenode). The following antibody was used: H3K27ac (ab4729, Abcam). 2 µg of antibody was used for each ChIP. The input DNA was precleared with protein G Dynabeads (Life Technologies) for 1 hour at 4°C and then incubated with antibodies conjugated protein G beads overnight at 4°C. The beads were then washed three times before elution of the bound DNA. Whole-genome amplification was performed on the eluted DNA using the WGA4 kit (Sigma-Aldrich) and BpmI-WGA primers. Amplified DNA was digested with BpmI(NEB). 30 ng of the amplified DNA was used to prepare libraries using the NEBNext ChIP-seq library preparation kit (NEB). ChIP-Seq in cell lines was also performed as described above but with 1 million cells. Each library (including matching input DNA) was sequenced to an average depth of 20–30 million raw reads on Illumina HiSeq4000 sequencer.

### ChIP-Seq data processing

Reads were quality-checked using FastQC. Adapter sequences were trimmed using Trimmomatic, and all reads were trimmed at the front and back by 10 bp. Reads were aligned to the hs37d5 human genome using bwa mem. Alignments with MAPQ<10 and duplicates were discarded. ChIP-Seq quality was checked using Phantompeakqualtools on the resulting bam files.

We called H3K27ac peaks using macs2 callpeak, with the parameters—nomodel—extsize 150 g hs—p=0.001. For each sample, a matching control sample (input DNA) was used. Peaks contained completely within problematic regions were removed (blacklist obtained from <https://mitra.stanford.edu/kundaje/akundaje/release/blacklists/hg19-human/>). We separated peaks into promoter peaks and enhancer peaks. Transcription start sites were obtained from UCSC RefSeq, and promoter regions were defined as TSS±2.5 kbp. Peaks inside promoter regions were defined as promoter peaks, and peaks outside promoter regions were defined as enhancer peaks. Peaks that crossed

promoter region boundaries were kept only if the remaining peak within their respective promoter or enhancer regions were >150 bp. Run-time commands and parameters are provided in the included scripts.

### ChIP-Seq data analysis

ChIP-Seq data analysis was performed in R, primarily using the DiffBind R package. Consensus enhancers, defined as enhancer peaks present in at least 2 samples, were used for analysis.

To map enhancers to target genes, we calculated the correlation between enhancer signals and gene expression levels. Here, enhancer signal was obtained using its DiffBind DBA\_SCORE\_READS\_MINUS score divided by the log of the enhancer width, followed by rank transformation. A gene's expression level was defined as its rank-transformed RNA-seq TPM value. The Spearman correlation was calculated between each enhancer and genes with transcription start sites located within ±Mbp, and genes with p<0.05 and r≥0.3 were kept as the target genes (allowing multiple target genes per enhancer). To validate the enhancers' target genes, we calculated the genes' promoter H3K27ac signals (similar to calculating enhancer signals), and calculated the correlation between the enhancers' H3K27ac levels and their derived targets' promoter H3K27ac levels, and found more than 80% of enhancer-target correlations were >0 (online supplemental figure S2A). As a sanity check, we also noted a significant correlation between the correlations of enhancer H3K27ac and target gene expression, and the correlations of enhancer H3K27ac and target promoter H3K27ac, indicating that enhancer-target pairs with higher enhancer-target gene expression linkage also had higher enhancer-target promoter activation linkage. The average distance between an enhancer and its target gene was 348.9 kbp, with more than half of enhancer-target distances <300 kbp, and 75% falling between 100 and 600 kbp (online supplemental figure S2A).

To cluster the enhancer profiles of CCA samples, we used hierarchical clustering (called from the dba.plotHeatmap method), with DiffBind's default scoring method (DBA\_SCORE\_TMM\_MINUS\_FULL), distMethod=spearman, maxSites=2000, hclustfun=ward.D2, to obtain the three enhancer groups (figure 1A). To validate this clustering, we performed consensus clustering using the ConsensusClusterPlus package, with maxK=10, reps=1000, pItem=0.9, pFeature=0.9, clusterAlg='hc', distance='spearman', innerLinkage='ward.D2', finalLinkage = 'ward.D2'. Plotting the change under the CDF curve revealed an elbow for k=7, and samples within each of the three enhancer groups were clustered together almost all the time in the consensus clusters (92.5% on average, online supplemental figure S2C), so we used the three enhancer groups for further analysis. We also plotted the first two PCs of enhancer profiles (using the rank-transform of enhancer signals) and observed that the three enhancer groups as well as the normal samples could be distinguished within the first two PCs (online supplemental figure S2B).

We performed differential binding analysis using DiffBind's dba.analyse method, with method=DBA\_DESEQ2, bFullLibrarySize=F, scoring method=DBA\_SCORE\_TMM\_MINUS\_FULL.

Run-time commands and parameters are provided in the included R scripts.

### Analysis pipeline to derive and validate somatic enhancers

We developed an analysis pipeline to derive and validate somatically gained or lost enhancers specific to each CCA enhancer group, and their respective enriched gene sets (online

supplemental figure S3). We noted that gene set enrichment analysis using Fisher's test versus GSEA can capture complementary or corroborating enriched gene sets and were therefore motivated to apply both methods to combine their results. The pipeline consisted of two complementary parts: first, to derive discrete somatic genes to find enriched gene sets using Fisher's test; second, to derive somatic-scored gene lists to find enriched gene sets using GSEA (which uses scored gene lists rather than discrete genes). To explain the pipeline here, we use an example of deriving somatic-gained enhancers specific to the ESTRO enhancer group.

Deriving discrete somatic genes and genesets: First, we derived enhancers gained in the ESTRO group versus the normal samples (ie, somatic gained enhancers,  $FDR < 0.05$ ) and gained in the ESTRO group versus the OXPHO group ( $FDR < 0.05$ ). Among these enhancers, we kept only those validated by gene expression, that is, those whose genes were upregulated in the ESTRO group versus the normal samples ( $p < 0.05$ ) and upregulated in the ESTRO group versus the OXPHO group ( $p < 0.05$ ). To remove enhancers that may be gained in the tumour microenvironment instead of in the tumour cells, we further kept only enhancers present in fluke-positive tumour cell-lines (enhancer level in the ESTRO group is in the top 50% of enhancer levels among the tumour cell-lines, where enhancer level was calculated as the concentration per log-width of the enhancer; we use fluke-positive cell-lines, since the ESTRO group is primarily fluke-positive). Among the remaining enhancers, we kept only those validated in fluke-positive tumour cell-lines, by keeping those also gained in the fluke-positive tumour cell-lines versus the normal cell-lines ( $\log\text{-foldchange} > 0.2$ ). The final remaining enhancers were those somatic-gained in the ESTRO group versus the OXPHO group. Then, the entire process was repeated, this time to derive somatic-gained enhancers in the ESTRO group versus the IMMUN group. We then took the intersection of these two groups of enhancers (somatic-gained in ESTRO vs OXPHO, and somatic-gained in ESTRO vs IMMUN), to define the somatic-gained enhancers specific to the ESTRO group. We performed geneset enrichment using Fisher's test ( $FDR < 0.05$ , MSigDB Hallmarks reference genesets). Somatic-lost enhancers specific to the ESTRO group, and their enriched genesets, were derived analogously.

Deriving somatic-scored gene lists and genesets: First, we derived the enhancer fold-change in the ESTRO group versus the normal group, the enhancer fold-change in the ESTRO group versus the OXPHO group, and the enhancer fold-change in the ESTRO group versus the IMMUN group. The enhancer somatic score was set to the weakest of these three fold-changes; if any of the three fold-changes were in opposite directions (eg, enhancer gain vs normal and OXPHO, but enhancer lost vs IMMUN), then the somatic score was set to 0. Thus, the enhancer somatic score reflects either a gain or loss of the enhancer in the ESTRO group relative to normal samples and the other groups. Next, we filtered by expression: if any of the expression changes of the ESTRO group versus normal samples, versus OXPHO group or versus IMMUN group, was in the opposite direction as the enhancer somatic score (eg, if the enhancer somatic score reflected gain in the ESTRO group, but an expression change reflected a downregulation in the ESTRO group), then the somatic score was set to 0. Next, for enhancers whose somatic score reflected a gain in ESTRO, to filter enhancers that may be gained in the tumour microenvironment instead of in the tumour cells, we set the enhancer somatic score to 0 if the enhancer was not present in fluke-positive tumour cell-lines (enhancer level in the ESTRO group was in the bottom 50% of enhancer levels

among the tumour cell-lines, where enhancer level was calculated as the concentration per log-width of the enhancer; we used fluke-positive cell-lines, since the ESTRO group was primarily fluke-positive; analogously for enhancers whose somatic scores reflected a loss in ESTRO). Next, we filtered by validation in tumour cell-lines: if the enhancer fold-change in fluke-positive tumour cell-lines versus normal cell-lines was in the opposite direction as the enhancer somatic score, then the somatic score was set to 0. The final remaining list of enhancers' somatic scores therefore reflected each enhancer's gain or loss in the ESTRO group relative to the normal samples and the OXPHO and IMMUN groups, where the score is 0 if expression changes or cell-line enhancer changes were not concordant with this gain or loss. We performed geneset enrichment using GSEA on this scored list ( $FDR < 0.05$ , MSigDB Hallmarks reference genesets).

Note that this analysis was agnostic to the possibility that differences between enhancer groups could be due to differences in their respective cells of origin; in this case, these differences are biologically relevant, and will be picked up in our analysis. Second, we acknowledge that what we termed somatically gained or lost enhancers are somatic with respect to our normal controls, which are bile duct tissues likely composed of mostly mature cholangiocytes; while in reality some CCAs may have developed from cholangiocytes at different developmental stages. However, without prior knowledge of the cells of origin of each CCA needed to pinpoint the exact somatic enhancers, we note that using mature bile duct tissues as our normal controls can perform well enough to derive biologically valid findings. Indeed, we also functionally and biologically validated any findings from the enhancer landscape in *in vitro* and *in vivo* models.

Run-time commands and parameters are provided in the included R scripts.

### ChIP-Seq signal tracks visualisation

To generate ChIP-Seq signal tracks visualisation, we first generated library-size-normalised, input-subtracted pileups using macs2 pileup and bdgcmp. Next, we normalised each sample's pileup using its DESEQ2 normalisation factor derived from DiffBind. The resulting file was converted to BigWig format and visualised on the UCSC genome browser. Run-time commands and parameters are provided in the included scripts. Representative samples were chosen for visualisation in the figures.

### DNA extraction and DNA methylation profiling microarray

Genomic DNA was extracted using DNeasy Blood and Tissue Kit (Qiagen). Sequencing libraries were prepared from DNA extracted using the SureSelect XT2 Target Enrichment System for the Illumina Multiplexed Sequencing platform (Illumina) according to the manufacturer's instructions. Whole genome sequencing was performed on Illumina HiSeq4000 sequencer. Infinium MethylationEPIC Kit (Illumina) was used for methylation profiling and performed according to the manufacturer's protocol.

### DNA methylation profile data analysis

We analysed DNA methylation data for 150 CCA samples, of which 138 were previously generated by Jusakul *et al*<sup>4</sup> (Infinium 450k BeadChip), and 12 were newly generated (Infinium MethylationEPIC BeadChip). We also included 11 normal samples. Data from the two assays were combined by using only their common probes and processed using only their minfi and watermelon packages. We performed unsupervised clustering with

the RPMM package, using the top 5000 CpG probes with the highest SD.

To analyse the relationship between enhancer gain/lost and DNA hypo/hypermethylation, we only considered enhancers that contained CpG islands or shores (since these are the genomic regions believed to be functionally affected by DNA methylation). An enhancer in a group (ESTRO, OXPHO or IMMUN) was considered hypermethylated if any of its contained CpG probes' M-values was significantly different between the group samples and the normal samples (T-test FDR<0.05), with a mean  $\beta$  difference>0.2 (analogously for hypomethylated). To analyse methylation within the CpG island/shore topology, we considered only CpG islands containing at least one island and one shore probe, where at least 75% of the probes are unmethylated in normal (mean  $\beta$ <0.3). For each cluster, we kept the CpG island/shore containing at least one hypermethylated probe and calculated the mean  $\beta$ -values in the CpG islands and shores in each sample in the cluster. To investigate genomic regions impacted by DNA hypermethylation, we annotated CpG islands/shores with chromatin states for liver and stomach tissues (data obtained from the 15\_coreMarks\_mnemonics files from Encode). For the Blue cluster (island-methylated), we calculated the chromatin-states-composition of island-methylated CpG islands. For the red cluster (shore-methylated), we calculated the chromatin-states-composition of shore-methylated CpG islands. This was done analogously for HCC and STAD.

Run-time commands and parameters are provided in the included scripts.

#### WGS variant calling and mutation signatures analysis

We performed variant calling with paired normal samples by using Strelka and Freebayes, and took their intersection to obtain higher confidence calls. We performed mutation signatures analysis using the mSigAct tool with the PCAWG mutational signatures which have been reported to occur in our tumour-type of interest, but removed the MSI, BRCA and POLE signatures.

#### Drug inhibition assays

A total of 1000 cells were seeded per well in a 96 well plate. One day after seeding, the indicated drug concentration were added to the cells. Cell proliferation was measured using Cell-Titer-Glo Luminescent Cell Viability Assay (Promega) for the indicated days after drug addition, according to manufacturer's protocol. IC<sub>50</sub> was determined using Graphpad Prism software. Drugs used were Rapamycin (TargetMol, T1537), Everolimus (TargetMol, T1784), IACS-010759 (TargetMol, T5337), Mubritinib (TargetMol, T6124) and Aristolochic Acid I (Sigma Aldrich, A5512).

#### Mouse xenograft and drug dosing

ARRIVE reporting guidelines 2.0<sup>91</sup> were used. All animal studies were conducted in compliance with animal protocols approved by Institutional Animal Care and Use Committee (IACUC) of Singapore (IACUC Ref. No.: 2018/SHS/1371) and of China (IACUC Ref No: SYSU-IACUC-2023-000318). Male NOD scid gamma mouse (NSG mice) (Jackson Lab, at least 8 weeks old) were implanted with  $1 \times 10^6$  cells subcutaneously. For PDX, tumours were placed in RPMI solution and cut into rough 5–20 mm<sup>3</sup> fragments. Rough 100 mm<sup>3</sup> of the cut tumour pieces were implanted subcutaneously into female mice (Jackson Lab, at least 8 weeks old). After the subcutaneous implanted tumours reach a calculated average volume of 50–100 mm<sup>3</sup>, the mice (minimum 30 g in weight) were randomised into three treatment

groups: (1) vehicle control, (2) low drug dose and (3) high drug dose. The dose of the drugs used were indicated in the respective figure legends. Everolimus (TargetMol, T1785) was dissolved in 10% DMSO and 10% corn oil (Targetmol, T5137). IACS-010759 (TargetMol, T5337) was dissolved in 0.5% methyl cellulose (Sigma). Both drugs were dosed by oral gavage once daily for five consecutive days a week (5 on, 2 off). Confounders such as the order of treatments and measurements, or animal/cage location were not controlled. Experiments cannot be blinded because experiments were performed by a single experimentalist. Five mice were housed per cage. The mice were provided with food and water ad libitum and monitored for changes in general health daily. Tumour volume was monitored every 3–4 days. Tumour volume was calculated as (length×width×width) $\times\pi/6$ ; the tumour volume of each group was computed as mean and SEM. P values were calculated using Students' t-test, using Microsoft Excel. Animals were sacrificed when the total tumour volume on both flanks exceeded 2000 mm<sup>3</sup>. The sample size was decided using statistical powering of type II error, with at least 6 mice used for each group.

#### OCR and glycolysis stress test

A total of 10 000 cells were plated in the Seahorse XFe96 96-well miniplates (Agilent) 1 day before each group was assay. After overnight incubation, cells were washed and medium was replaced with the recommended Seahorse Mitostress basal media and placed in a CO<sub>2</sub>-free 37°C incubator for 1 hour. OCR was then measured by the Seahorse XFe96 Analyzer (Agilent) according to the manufacturer's protocol. BCA protein quantification (ThermoFisher Scientific) was used to measure protein concentration after the assays and used for normalisation purposes.

#### MitoTracker Green FM and Red CMXRos staining

Cells were incubated with media containing MitoTracker Green FM (ThermoFisher, M7514), MitoTracker Red CMXRos (ThermoFisher Scientific, M7512) and Hoechst 33342 (ThermoFisher Scientific, 62249) for 1 hour and then replaced with normal media. Images were acquired by confocal microscope (Zeiss LSM700).

#### Immunoblotting

Collected cell pellets were lysed in RIPA buffer supplemented with protease and phosphatase inhibitor cocktail for whole cell protein lysate immunoblotting (Roche). At least 20 µg of protein was used for each immunoblotting experiment. Proteins were transferred to PVDF membranes. Western blotting was performed by incubating membranes overnight at 4°C with the following antibodies: P-P70 S6K Thr389 (Cell Signaling, 9234), P70 S6K (Cell Signaling, 9202), P-AKT Ser473 (Cell Signaling, 9271), AKT (Cell Signaling, 9272), OxPhos Human WB Antibody Cocktail (ThermoFisher Scientific, 45-8199) and Tubulin (Proteintech, 66240). The bands were detected with SuperSignal West Femto Maximum Sensitivity Substrate (ThermoFisher Scientific).

#### Multiplex immunohistochemical staining (Vectra)

Vectra was performed and analysed as previously described.<sup>27–29</sup> Multiplex immunohistochemistry staining was performed on 4 µm thick formalin-fixed paraffin-embedded (FFPE) human scalp tissue sections using Leica Bond Max autostainer (Leica Biosystems), Bond Refine Detection Kit (Leica Biosystems) and

Opal 6-Plex Detection Kit—for Whole Slide Imaging (Akoya Biosciences).

In brief, FFPE tissue sections were subjected to repeated cycles of heat-induced epitope retrieval, incubation with primary antibodies, secondary antibodies (Bond Refine Kit) and Opal tyramide signal amplification (Akoya Bioscience). The primary antibodies used were PD-L1 (Cell Signaling Technology, 13 684S), CS56 (Leica Biosystems, NCL-L-CD56-504), PD-L2 (Cell Signaling Technology, 82 723S), CD68 (Dako, M0876), CD8 (Leica Biosystems, NCL-L-CD8-4B11), FOXP3 (Abcam, ab20034). After all six markers had been applied, spectral DAPI (Akoya Bioscience) was then applied as the nuclear counterstain.

Images were captured using the Vectra 3 Automated Quantitative Pathology Imaging System (Akoya Biosciences), and analysed using the HALO Image Analysis Platform (Indica Labs).

### NanoString

NanoString PanCancer IO360<sup>TM</sup> panel (NanoString Technologies, Seattle, Washington, USA) was used as per manufacturer's protocol using the nCounter platform. RNA extracted from frozen tumours were checked using the 2100 Bioanalyzer (Agilent Technologies, Palo Alto, California, USA) for quality before use. The obtained NanoString data were analysed on the nSolver V.4.0 Advanced Analysis module using default settings to obtain differentially expressed genes, pathway scores and cell-type scores.

### Visium spatial transcriptomics

Flash frozen tissues were cryosectioned and placed on a Visium gene expression slide (10x Genomics). H&E staining, permeabilisation, reverse transcription, second strand synthesis and cDNA amplification was performed using the Visium Spatial Gene Expression Reagent Kit (10X genomics) as per the manufacturer's instructions. Library Construction Kit (10x genomics) and Dual Index Kit TT Set A (10x genomics) were used to make dual indexed libraries from the amplified cDNA as per the manufacturer's instructions. The libraries were sequenced on the Novaseq 6000 instrument (Illumina). 10X Space Ranger V.1.3.1 (10x genomics) with the default parameters was used to map the reads against that hg38 reference genome. BayesSpace (V.3.17)<sup>31</sup> with k=4 was used to cluster the mapped reads. VarTrix (10x genomics) and somatic mutation data from bulk whole genome sequencing data was used to perform mutation signature analysis on Visium data. CITE-seq PBMC data (in Seurat V.4.0 package),<sup>33 34</sup> Seurat V.4.0 and MCP-counter<sup>32</sup> were used to map and identify immune cell populations.

### Author affiliations

- <sup>1</sup>Cancer and Stem Cell Biology Programme, Duke-NUS Medical School, Singapore
- <sup>2</sup>Laboratory of Cancer Epigenome, National Cancer Centre Singapore, Singapore
- <sup>3</sup>Department of Computer Science, National University of Singapore, Singapore
- <sup>4</sup>Division of Medical Oncology, National Cancer Centre Singapore, Singapore
- <sup>5</sup>Cancer Discovery Hub, National Cancer Centre Singapore, Singapore
- <sup>6</sup>Oncology Academic Clinical Program, Duke-NUS Medical School, Singapore
- <sup>7</sup>Singapore Immunology Network, Agency for Science Technology and Research (A\*STAR), Singapore
- <sup>8</sup>Bioinformatics Institute (BII), Agency for Science Technology and Research (A\*STAR), Singapore
- <sup>9</sup>State Key Laboratory of Oncology in South China, Collaborative Innovation Center of Cancer Medicine, Sun Yat-sen University Cancer Center, Guangzhou, China
- <sup>10</sup>Genome Institute of Singapore, Agency for Science Technology and Research (A\*STAR), Singapore
- <sup>11</sup>Centre for Computational Biology, Duke-NUS Medical School, Singapore
- <sup>12</sup>Institute of Molecular and Cell Biology, Agency for Science Technology and Research (A\*STAR), Singapore
- <sup>13</sup>Institute of Molecular and Cell Biology, Integrative Biology for Theranostics Lab, Agency for Science Technology and Research (A\*STAR), Singapore

<sup>14</sup>Cholangiocarcinoma Screening and Care Program (CASCAP), Khon Kaen University, Khon Kaen, Thailand

<sup>15</sup>Department of Biochemistry, Faculty of Medicine, Khon Kaen University, Khon Kaen, Thailand

<sup>16</sup>Department of Liver Surgery, Sun Yat-Sen University Cancer Center, Guangzhou, Guangdong

<sup>17</sup>Department of Pancreaticobiliary Surgery, Sun Yat-sen University, Guangzhou, China

<sup>18</sup>Department of Pathology, Faculty of Medicine, Khon Kaen University, Khon Kaen, Thailand

<sup>19</sup>Center of Digestive Diseases and Liver Transplantation, Fundeni Clinical Institute, Bucuresti, Romania

<sup>20</sup>Department of Gastroenterology and Hepatology, Chang Gung Memorial Hospital and Chang Gung University, Taoyuan, Taiwan

<sup>21</sup>Department of General Surgery, Chang Gung Memorial Hospital and Chang Gung University, Taoyuan, Taiwan

<sup>22</sup>Department of Anatomical Pathology, Singapore General Hospital, Singapore

<sup>23</sup>Pathology Academic Clinical Program, Duke-NUS Medical School, Singapore

<sup>24</sup>Cholangiocarcinoma Research Institute, Khon Kaen University, Khon Kaen, Thailand

<sup>25</sup>Department of Pharmacology, Faculty of Medicine, Khon Kaen University, Khon Kaen, Thailand

<sup>26</sup>Centre for Research and Development of Medical Diagnostic Laboratories, Faculty of Associated Medical Sciences, Khon Kaen University, Khon Kaen, Thailand

<sup>27</sup>Cancer Science Institute of Singapore, National University of Singapore, Singapore

<sup>28</sup>State Key Laboratory of Oncology, Collaborative Innovation Center of Cancer Medicine, Sun Yat-sen University Cancer Center, Guangzhou, China

**Acknowledgements** We are grateful to Professor Donald McDonnell from Duke University School of Medicine, USA for his suggestions and advice. We would like to thank Duke-NUS Genome Biology Facility (DGBF) of Duke-NUS Medical School, Auristone Pte Ltd and Cancer Discovery Hub (CDH) of National Cancer Centre Singapore for their services. We would also like to thank the Verdant Foundation for their support. This manuscript is dedicated to the memory of Professor Narong Khuntikeo and Professor Vajarabhongsa Bhudhiswasdi from Khon Kaen University, Thailand.

**Contributors** JHH and CHY contributed equally to this manuscript.

Conceptualisation: JHH, CHY and BTT; Writing of original draft: JHH and CHY; Writing (review and editing): JHH, CHY, BTT, JT, JYC, SK, AJ, JY, FYTW, JCTL and PG; Supervision: BTT; Experiments: JHH, CHY, HLH, JC, JYL, ZL, PLC, SRN, PW, XR, XZ, YS, WL, JK, FYTW, JCTL and XYK; Analysis: JHH, CHY, HLH, JYC, MCL, AB, AHL, PG, XY, FYTW, JCTL and JY; Resources and intellectual discussion: HLH, CCYN, PK, YZ, JL, WMDT, CP, SD, IP, S-YH, M-CY, JY, SK, AJ, WL, PT, JT and BTT; Approval of final version of manuscript: all authors. Guarantor: BTT.

**Funding** JHH was supported by the National Research Medical Council Singapore Young Individual Research Grant (MOH-000232 and COVIDTUG21-0087), the Khoo Postdoctoral Fellowship Award (Duke-NUS-KPFA/2019/0034) and the Singapore Therapeutics Development Review Pre-Pilot (H23G1a0009). CHY was supported by the SingHealth Academic Medicine (AM) Research Grant (AM/SU021/201). JT was supported by the National Natural Science Foundation of PR. China (81972596, 81772963, 82320108015 and 81773279), the Natural Science Foundation of Guangdong Province, China (2021A1510011131) and the National Key R&D Program of China (2022YFA1304000). BTT was supported by the National Medical Research Council Singapore Translational Research Investigator Award (MOH000248-00), the National Medical Research Council Open Fund-Individual Research Grant (MOH-000144 and COVID19TUG21-0146), the Verdant Foundation and the NCC Cancer Fund.

**Competing interests** None declared.

**Patient and public involvement** Patients and/or the public were not involved in the design, or conduct, or reporting, or dissemination plans of this research.

**Patient consent for publication** Not applicable.

**Ethics approval** Signed informed consent was obtained from patients. The study was approved by the SingHealth Centralised Institutional Review Board (2006/449/B), Khon Kaen University (HE471214), Linkou Chang Gung Memorial Hospital (100-2030B) and Ethics Committee of the Clinical Institute of Digestive Diseases and Liver Transplantation, Fundeni (215/18.01.2010).

**Provenance and peer review** Not commissioned; externally peer reviewed.

**Data availability statement** Data are available in a public, open access repository. Sequencing datasets can be found at the European Genome-phenome Archive (EGA, Accession number: EGAS00001007309). Data used in this manuscript also includes previously published studies from public repositories: EGA (EGA00001000950) and Gene Expression Omnibus (GEO, GSE89749 and GSE89803). Codes used are available on GitHub ([https://github.com/chernycherny/CCA\\_enhancers\\_2023](https://github.com/chernycherny/CCA_enhancers_2023)).

**Supplemental material** This content has been supplied by the author(s). It has not been vetted by BMJ Publishing Group Limited (BMJ) and may not have been peer-reviewed. Any opinions or recommendations discussed are solely those of the author(s) and are not endorsed by BMJ. BMJ disclaims all liability and responsibility arising from any reliance placed on the content. Where the content includes any translated material, BMJ does not warrant the accuracy and reliability of the translations (including but not limited to local regulations, clinical guidelines, terminology, drug names and drug dosages), and is not responsible for any error and/or omissions arising from translation and adaptation or otherwise.

#### ORCID iDs

Jing Han Hong <http://orcid.org/0000-0002-2173-9192>  
 Sheng Rong Ng <http://orcid.org/0000-0003-1655-2443>  
 Joe Yeong <http://orcid.org/0000-0002-6674-7153>  
 Patrick Tan <http://orcid.org/0000-0002-0179-8048>  
 Jing Tan <http://orcid.org/0000-0002-4605-4624>  
 Bin Tean Teh <http://orcid.org/0000-0003-1514-1124>

#### REFERENCES

- 1 Kam AE, Masood A, Shroff RT. Current and emerging therapies for advanced biliary tract cancers. *Lancet Gastroenterol Hepatol* 2021;6:956–69.
- 2 Abou-Alfa GK, Sahai V, Hollebecque A, et al. Pemigatinib for previously treated, locally advanced or metastatic cholangiocarcinoma: a multicentre, open-label, phase 2 study. *Lancet Oncol* 2020;21:671–84.
- 3 Zhu AX, Macarulla T, Javle MM, et al. Final results from claridhy, a global, phase III, randomized, double-blind study of Ivsosidenib (IVO) versus placebo (PBO) in patients (Pts) with previously treated cholangiocarcinoma (CCA) and an Isocitrate dehydrogenase 1 (Idh1) Mutation. *JCO* 2021;39(3\_suppl):266.
- 4 Jusakul A, Cutcutache I, Yong CH, et al. Whole-genome and epigenomic landscapes of etiologically distinct subtypes of cholangiocarcinoma. *Cancer Discov* 2017;7:1116–35.
- 5 Kongpetch S, Jusakul A, Lim JQ, et al. Lack of targetable Fgfr2 fusions in endemic fluke-associated cholangiocarcinoma. *JCO Glob Oncol* 2020;6:628–38.
- 6 Chan-On W, Nairismägi M-L, Ong CK, et al. Exome sequencing identifies distinct mutational patterns in liver fluke-related and non-infection-related bile duct cancers. *Nat Genet* 2013;45:1474–8.
- 7 Farshidfar F, Zheng S, Gingras M-C, et al. Integrative genomic analysis of cholangiocarcinoma identifies distinct IDH-mutant molecular profiles. *Cell Rep* 2017;19:2878–80.
- 8 Lin CY, Erkek S, Tong Y, et al. Active Medulloblastoma enhancers reveal subgroup-specific cellular origins. *Nature* 2016;530:57–62..
- 9 Mack SC, Pajtler KW, Chavez L, et al. Therapeutic targeting of ependymoma as informed by oncogenic enhancer profiling. *Nature* 2018;553:101:101–5..
- 10 Morrow JJ, Bayles I, Funnell APW, et al. Positively selected enhancer elements endow osteosarcoma cells with metastatic competence. *Nat Med* 2018;24:525.
- 11 Yao X, Tan J, Lim KJ, et al. VHL deficiency drives enhancer activation of oncogenes in clear cell renal cell carcinoma. *Cancer Discov* 2017;7:1284–305.
- 12 Alayev A, Salomon RS, Berger SM, et al. Mtorc1 directly phosphorylates and activates ER $\alpha$  upon estrogen stimulation. *Oncogene* 2016;35:3535–43.
- 13 Alvaro D, Barbaro B, Franchitto A, et al. Estrogens and insulin-like growth factor 1 modulate neoplastic cell growth in human cholangiocarcinoma. *Am J Pathol* 2006;169:877–88.
- 14 Hunsawong T, Singsuksawat E, In-chon N, et al. Estrogen is increased in male cholangiocarcinoma patients' serum and stimulates invasion in cholangiocarcinoma cell lines in vitro. *J Cancer Res Clin Oncol* 2012;138:1311–20.
- 15 Mancino A, Mancino MG, Glaser SS, et al. Estrogens stimulate the proliferation of human cholangiocarcinoma by inducing the expression and secretion of vascular endothelial growth factor. *Dig Liver Dis* 2009;41:156–63.
- 16 Marziona M, Torrice A, Saccomanno S, et al. An oestrogen receptor B-selective agonist exerts anti-neoplastic effects in experimental Intrahepatic cholangiocarcinoma. *Dig Liver Dis* 2012;44:134–42.
- 17 Singsuksawat E, Thuwajit C, Charngkaew K, et al. Increased Etv4 expression correlates with estrogen-enhanced proliferation and invasiveness of cholangiocarcinoma cells. *Cancer Cell Int* 2018;18:25.
- 18 Sritana N, Suriyo T, Kanithayanun J, et al. Glyphosate induces growth of estrogen receptor alpha positive cholangiocarcinoma cells via non-Genomic estrogen receptor/Erk1/2 signaling pathway. *Food Chem Toxicol* 2018;118:595–607.
- 19 Tanjak P, Thiantanawat A, Watcharasit P, et al. Genistein reduces the activation of AKT and EGFR, and the production of IL6 in cholangiocarcinoma cells involving estrogen and estrogen receptors. *Int J Oncol* 2018;53:177–88.
- 20 Welboren W-J, Stunnenberg HG, Sweep FCGJ, et al. Identifying estrogen receptor target genes. *Mol Oncol* 2007;1:138–43.
- 21 Yang W, Schwartz GN, Marotti JD, et al. Estrogen receptor alpha drives Mtorc1 inhibitor-induced feedback activation of PI3K/AKT in ER+ breast cancer. *Oncotarget* 2018;9:8810–22.
- 22 Klawitter J, Nashan B, Christians U. Everolimus and sirolimus in transplantation-related but different. *Expert Opin Drug Saf* 2015;14:1055–70.
- 23 Baccelli I, Gareau Y, Lehnertz B, et al. Muritribulin targets the electron transport chain complex I and reveals the landscape of OXPHOS dependency in acute myeloid leukemia. *Cancer Cell* 2019;36:84–99.
- 24 Baran N, Lodi A, Dhungana Y, et al. Inhibition of mitochondrial complex I reverses Notch1-driven metabolic reprogramming in T-cell acute lymphoblastic leukemia. *Nat Commun* 2022;13:2801.
- 25 Molina JR, Sun Y, Protopopova M, et al. An inhibitor of oxidative phosphorylation exploits cancer vulnerability. *Nat Med* 2018;24:1036–46.
- 26 Torrey H, Butterworth J, Mera T, et al. Targeting Tnfr2 with antagonistic antibodies inhibits proliferation of ovarian cancer cells and tumor-associated Tregs. *Sci Signal* 2017;10:eaaf8608.
- 27 Lim JCT, Yeong JPS, Lim CJ, et al. An automated staining protocol for seven-colour Immunofluorescence of human tissue sections for diagnostic and prognostic use. *Pathology* 2018;50:333–41.
- 28 Yeong J, Lim JCT, Lee B, et al. High densities of tumor-associated plasma cells predict improved prognosis in triple negative breast cancer. *Front Immunol* 2018;9:1209.
- 29 Yeong J, Thike AA, Lim JCT, et al. Higher densities of Foxp3(+) regulatory T cells are associated with better prognosis in triple-negative breast cancer. *Breast Cancer Res Treat* 2017;163:21–35.
- 30 Lu ZN, Luo Q, Zhao LN, et al. The mutational features of aristolochic acid-induced Mouse and human liver cancers. *Hepatology* 2020;71:929–42.
- 31 Zhao E, Stone MR, Ren X, et al. BayesSpace enables the robust characterization of spatial gene expression architecture in tissue sections at increased resolution. *Bioinformatics* [Preprint].
- 32 Becht E, Giraldo NA, Lacroix L, et al. Estimating the population abundance of tissue-infiltrating immune and stromal cell populations using gene expression. *Genome Biol* 2016;17:249:249..
- 33 Hao Y, Hao S, Andersen-Nissen E, et al. Integrated analysis of multimodal single-cell data. *Cell* 2021;184:3573–3587.
- 34 Pont F, Tosolini M, Gao Q, et al. Single-cell virtual cytometer allows user-friendly and versatile analysis and visualization of multimodal single cell RNAseq Datasets. *NAR Genom Bioinform* 2020;2:lgaa025.
- 35 Calo E, Wysocka J. Modification of enhancer chromatin: what, how, and why? *Mol Cell* 2013;49:825–37.
- 36 Roadmap Epigenomics Consortium, Kundaje A, Meuleman W, et al. Integrative analysis of 111 reference human epigenomes. *Nature* 2015;518:317–30.
- 37 Ally A, Balasundaram M, Carlsen R, et al. Comprehensive and integrative genomic characterization of hepatocellular carcinoma. *Cell* 2017;169:1327–1341.
- 38 The Cancer Genome Atlas Research Network. Comprehensive molecular characterization of gastric adenocarcinoma. *Nature* 2014;513:202–9.
- 39 Thorsson V, Gibbs DL, Brown SD, et al. The immune landscape of cancer. *Immunity* 2018;48:S1074–7613(18)30121-3:812–830..
- 40 Ong CK, Subimber C, Pairojkul C, et al. Exome sequencing of liver fluke-associated Cholangiocarcinoma. *Nat Genet* 2012;44:690–3.
- 41 Chaisaengmongkol J, Budhu A, Dang H, et al. Common molecular subtypes among Asian hepatocellular carcinoma and Cholangiocarcinoma. *Cancer Cell* 2017;32:S1535–6108(17)30205-2:57–70..
- 42 Lin J, Cao Y, Yang X, et al. Mutational spectrum and precision oncology for biliary tract carcinoma. *Theranostics* 2021;11:4585–98.
- 43 Xue R, Chen L, Zhang C, et al. Genomic and transcriptomic profiling of combined hepatocellular and intrahepatic cholangiocarcinoma reveals distinct molecular subtypes. *Cancer Cell* 2019;35:S1535–6108(19)30202-8:932–947..
- 44 Zou S, Li J, Zhou H, et al. Mutational landscape of intrahepatic cholangiocarcinoma. *Nat Commun* 2014;5:5696.
- 45 An J, Kim D, Oh B, et al. Comprehensive characterization of viral integrations and genomic aberrations in HBV-infected intrahepatic cholangiocarcinomas. *Hepatology* 2022;75:997–1011.
- 46 Boerner T, Drill E, Pak LM, et al. Genetic determinants of outcome in intrahepatic cholangiocarcinoma. *Hepatology* 2021;74:1429–44.
- 47 Carapeto F, Bozorgui B, Shroff RT, et al. The immunogenomic landscape of resected intrahepatic cholangiocarcinoma. *Hepatology* 2022;75:297–308.
- 48 Goeppert B, Folseraas T, Roessler S, et al. Genomic characterization of cholangiocarcinoma in primary sclerosing cholangitis reveals therapeutic opportunities. *Hepatology* 2020;72:1253–66.
- 49 Song G, Shi Y, Meng L, et al. Single-cell transcriptomic analysis suggests two molecularly subtypes of intrahepatic Cholangiocarcinoma. *Nat Commun* 2022;13:1642.
- 50 Wang X-Y, Zhu W-W, Wang Z, et al. Driver mutations of Intrahepatic cholangiocarcinoma shape clinically relevant genomic clusters with distinct molecular features and therapeutic vulnerabilities. *Theranostics* 2022;12:260–76.
- 51 Zhang Y, Ma Z, Li C, et al. The Genomic landscape of cholangiocarcinoma reveals the disruption of post-transcriptional modifiers. *Nat Commun* 2022;13:3061.
- 52 Liu R, Dong J-T, Chen C. Role of Klf5 in hormonal signaling and breast cancer development. *Vitam Horm* 2013;93:213–25.

- 53 Nakajima Y, Akaogi K, Suzuki T, et al. Estrogen regulates tumor growth through a nonclassical pathway that includes the transcription factors ER $\beta$  and Klf5. *Sci Signal* 2011;4:ra22.
- 54 Nakajima Y, Osakabe A, Waku T, et al. Estrogen exhibits a Biphasic effect on prostate tumor growth through the estrogen receptor B-Klf5 pathway. *Mol Cell Biol* 2016;36:144–56.
- 55 Jia X, Chen H, Ren Y, et al. Bap1 antagonizes Wwp1-mediated transcription factor Klf5 ubiquitination and inhibits autophagy to promote melanoma progression. *Exp Cell Res* 2021;402:112506.
- 56 Gong T, Cui L, Wang H, et al. Knockdown of Klf5 suppresses hypoxia-induced resistance to cisplatin in NSCLC cells by regulating HIF-1A-dependent glycolysis through inactivation of the Pi3K/AKT/mTOR pathway. *J Transl Med* 2018;16:164.
- 57 Madak-Erdogan Z, Kim SH, Gong P, et al. Design of pathway preferential estrogens that provide beneficial metabolic and vascular effects without stimulating reproductive tissues. *Sci Signal* 2016;9:ra53.
- 58 Heits N, Heinze T, Bernsmeier A, et al. Influence of mTOR-inhibitors and mycophenolic acid on human cholangiocellular carcinoma and cancer associated fibroblasts. *BMC Cancer* 2016;16:322.
- 59 Lin G, Lin KJ, Wang F, et al. Synergistic antiproliferative effects of an mTOR inhibitor (Rad001) plus gemcitabine on cholangiocarcinoma by decreasing choline kinase activity. *Dis Model Mech* 2018;11:dmm033050.
- 60 Wu CE, Chen MH, Yeh CN. mTOR inhibitors in advanced biliary tract cancers. *Int J Mol Sci* 2019;20:500.
- 61 Li X, Lu J, Zhang L, et al. Clinical implications of monitoring Esr1 mutations by circulating tumor DNA in estrogen receptor positive metastatic breast cancer: A pilot study. *Transl Oncol* 2020;13:321–8.
- 62 Zhao X, Zhang C, Zhou H, et al. Synergistic antitumor activity of the combination of Salubrinal and rapamycin against human Cholangiocarcinoma cells. *Oncotarget* 2016;7:85492–501.
- 63 Gaudé E, Frezza C. Tissue-specific and CONVERGENT metabolic transformation of cancer correlates with metastatic potential and patient survival. *Nat Commun* 2016;7:13041.
- 64 Sriskanthadevan S, Jeyaraju DV, Chung TE, et al. AML cells have low spare reserve capacity in their respiratory chain that renders them susceptible to oxidative metabolic stress. *Blood* 2015;125:2120–30.
- 65 Stuani L, Sabatier M, Saland E, et al. Mitochondrial metabolism supports resistance to IDH mutant inhibitors in acute myeloid leukemia. *J Exp Med* 2021;218:e20200924.
- 66 Yap TA, Daver N, Mahendra M, et al. Complex I inhibitor of oxidative phosphorylation in advanced solid tumors and acute myeloid leukemia: phase I trials. *Nat Med* 2023;29:115–26.
- 67 Donati G, Nicoli P, Verrecchia A, et al. Oxidative stress enhances the therapeutic action of a respiratory inhibitor in MYC-driven lymphoma. *EMBO Mol Med* 2023;15:e16910.
- 68 Lin Z, Li J, Zhang J, et al. Metabolic reprogramming driven by Igf2Bp3 promotes acquired resistance to EGFR inhibitors in non-small cell lung cancer. *Cancer Research* 2023;83:2187–207.
- 69 Zheng Q, Zhang B, Li C, et al. Overcome drug resistance in cholangiocarcinoma: new insight into mechanisms and refining the Preclinical experiment models. *Front Oncol* 2022;12:850732.
- 70 Dickman KG, Chen CH, Grollman AP, et al. Aristolochic acid-containing Chinese Herbal medicine and upper urinary tract urothelial carcinoma in Taiwan: a narrative review. *World J Urol* 2023;41:899–907.
- 71 Poon SL, Pang S-T, McPherson JR, et al. Genome-wide mutational signatures of aristolochic acid and its application as a screening tool. *Sci Transl Med* 2013;5:197ra101.
- 72 Wang SM, Lai MN, Chen PC, et al. Increased upper and lower tract urothelial carcinoma in patients with end-stage renal disease: a nationwide cohort study in Taiwan during 1997–2008. *BioMed Research International* 2014;2014:1–9.
- 73 Klein O, Kee D, Nagrial A, et al. Evaluation of combination nivolumab and ipilimumab Immunotherapy in patients with advanced biliary tract cancers. *JAMA Oncol* 2020;6:1405.
- 74 Cadamuro M, Sarcognato S, Camerotto R, et al. Intrahepatic cholangiocarcinoma developing in patients with metabolic syndrome is characterized by osteopontin overexpression in the tumor stroma. *Int J Mol Sci* 2023;24:4748.
- 75 De Lorenzo S, Tovoli F, Mazzotta A, et al. n.d. Non-alcoholic steatohepatitis as a risk factor for intrahepatic cholangiocarcinoma and its Prognostic role. *Cancers*;12:3182.
- 76 Ghidini M, Ramai D, Facciorusso A, et al. Metabolic disorders and the risk of cholangiocarcinoma. *Expert Rev Gastroenterol Hepatol* 2021;15:999–1007.
- 77 Maeda S, Hikiba Y, Fujiwara H, et al. NAFLD exacerbates cholangitis and promotes cholangiocellular carcinoma in mice. *Cancer Sci* 2021;112:1471–80.
- 78 Xiao J, Ng CH, Chan KE, et al. Hepatic, extra-hepatic outcomes and causes of mortality in NAFLD - an umbrella overview of systematic review of meta-analysis. *J Clin Exp Hepatol* 2023;13:656–65.
- 79 Sirica AE, Gores GJ, Groopman JD, et al. Intrahepatic cholangiocarcinoma: continuing challenges and translational advances. *Hepatology* 2019;69:1803–15.
- 80 Fabris L, Sato K, Alpini G, et al. The tumor microenvironment in cholangiocarcinoma progression. *Hepatology* 2021;73 Suppl 1(Suppl 1):75–85.
- 81 Moghal N, Li Q, Stewart EL, et al. Single-cell analysis reveals Transcriptomic features of drug-tolerant persisters and stromal adaptation in a patient-derived EGFR-mutated lung adenocarcinoma xenograft model. *J Thorac Oncol* 2023;18:499–515.
- 82 Wang H, Li N, Liu Q, et al. Antiandrogen treatment induces stromal cell reprogramming to promote castration resistance in prostate cancer. *Cancer Cell* 2023;41:S1535–6108(23)00183–6:1345–1362..
- 83 Rastegar-Pouyani N, Montazeri V, Marandi N, et al. The impact of cancer-associated fibroblasts on drug resistance, stemness, and epithelial-mesenchymal transition in bladder cancer: a comparison between recurrent and non-recurrent patient-derived Cafs. *Cancer Invest* 2023;41:656–71.
- 84 Amin T, Viol F, Krause J, et al. Cancer-associated fibroblasts induce proliferation and therapeutic resistance to everolimus in neuroendocrine tumors through Stat3 activation. *Neuroendocrinology* 2023;113:501–18.
- 85 Duan Y, Zhang X, Ying H, et al. Targeting Mfp5 in cancer-associated fibroblasts sensitizes pancreatic cancer to PD-L1-based immunochemotherapy via remodeling the matrix. *Oncogene* 2023;42:2061–73.
- 86 Yoshida GJ. Applications of patient-derived tumor xenograft models and tumor organoids. *J Hematol Oncol* 2020;13:4.
- 87 Jelinek D, Zhang ER, Ambros A, et al. A mouse model to investigate the role of cancer-associated fibroblasts in tumor growth. *J Vis Exp* December 22, 2020.
- 88 Sripa B, Seubwai W, Vaeteewoottacharn K, et al. Functional and genetic characterization of three cell lines derived from a single tumor of an opisthorchis viverrini-associated cholangiocarcinoma patient. *Hum Cell* 2020;33:695–708.
- 89 Grubman SA, Perrone RD, Lee DW, et al. Regulation of intracellular pH by immortalized human intrahepatic biliary epithelial cell lines. *Am J Physiol* 1994;266(6 Pt 1):G1060–70.
- 90 Muratani M, Deng N, Ooi WF, et al. Nanoscale chromatin profiling of gastric adenocarcinoma reveals cancer-associated cryptic promoters and somatically acquired regulatory elements. *Nat Commun* 2014;5:4361.
- 91 Percie du Sert N, Hurst V, Ahluwalia A, et al. The ARRIVE guidelines 2.0: updated guidelines for reporting animal research. *Br J Pharmacol* 2020;177:3617–24.
- 92 Jusakul A, Cutcutache I, Yong CH, et al. Data from: whole Exome and Transcriptome sequencing of biliary tract cancer. 2016. Available: <https://ega-archive.org/studies/EGAS00001000950>
- 93 Jusakul A, Cutcutache I, Yong CH, et al. Data from: whole-genome and Epigenomic landscapes of Etiologically distinct subtypes of Cholangiocarcinoma. Gene Expression Omnibus, . 2017Available: <https://www.ncbi.nlm.nih.gov/geo/query/acc.cgi?acc=GSE89749>
- 94 Jusakul A, Cutcutache I, Yong CH, et al. Data from: whole-genome and Epigenomic landscapes of Etiologically distinct subtypes of Cholangiocarcinoma. Gene Expression Omnibus, . 2017Available: <https://www.ncbi.nlm.nih.gov/geo/query/acc.cgi?acc=GSE89803>